A numerical study of electron-magnetohydrodynamics tearing modes in parameter ranges of experimental interest

Homam Betar, Daniele Del Sarto, A. Ghizzo, F. Brochard, David Zarzoso

A numerical study of electron-magnetohydrodynamics tearing modes in parameter ranges of experimental interest

H. Betar,[1, 2, a)] D. Del Sarto,[3, b)] A. Ghizzo,[3, c)] F. Brochard,[3, d)] and D. Zarzoso[4, e)]
[1)]*Aix-Marseille Université, CNRS, Centrale Marseille, M2P2 UMR 7340 Marseille, France*
[2)]*Renaissance Fusion, 38600 Fontaine, France*
[3)]*Institut Jean Lamour, UMR 7198 CNRS – Université de Lorraine, F-54000 Nancy, France*
[4)]*Aix-Marseille Université, CNRS, Centrale Marseille, M2P2 UMR 7340 Marseille, France*

(Dated: 27 April 2024)

We perform a numerical study of the linear dynamics of tearing modes in slab incompressible electron-magnetohydrodynamics (EMHD) by considering some parameter ranges which can be of interest for laboratory plasmas (e.g., helicon devices) or for astrophysics (e.g., solar-wind turbulence). To this purpose several non-ideal effects are simultaneously retained (finite electron inertia, resistivity and electron viscosity) and we make distinction between the dissipation coefficients in the direction parallel and perpendicular to the guide field. We thus identify some new reconnection regimes, characterized by a departure from the customary monotonic power-law scalings of the growth rates with respect to the non-ideal parameters. The results here presented can provide a useful indication for future studies of EMHD regimes relevant to experiments and for extensions of the EMHD tearing mode modelling to more complete regimes including kinetic effects (e.g., "electron-only" reconnection in kinetic regimes).

I. INTRODUCTION

Electron magnetohydrodynamics (EMHD) is a reduced fluid model which describes the collective fluid dynamics of a barotropic electron plasma at non-relativistic phase-velocities and temperatures, and at scales at which the ion dynamics is completely neglected[1,2]. This paper employs the non-relativistic, incompressible 2D reduced EMHD model[3] derived for slab geometry under the assumption of a strong guide field along the z direction. In this regime the linear dynamics is governed by whistler waves. Accounting for compressibility in the model involves considering charge separation effects, which can become important when the magnetic field is large enough to make the whistler wave frequency comparable to the cyclotron frequency. Here we neglect these effects.

Magnetic reconnection (see, e.g., Ref. 4) is a process involving the collective response of particles in a plasmas, which implies a conversion of energy, from the "magnetic" component stored in the electromagnetic (e.m.) field to the kinetic component associated to the ordered and disordered motion of the charged particles. Magnetic reconnection is associated to a change of the so-called "magnetic topology" in the plasma, that is, the configuration of the magnetic lines in the plasma. This notion takes on a specific meaning in a plasma due to the linking which exists at the fluid scales between the magnetic lines and the averaged particle motion, because of the fact that a fluid parcel of the plasma is constrained not to depart, during its large scale dynamics, from the magnetic line it was initially bound to. A microscopic rearrangement of the linking between magnetic lines and a fluid plasma parcel is indeed allowed locally in time and in space by some "non-ideal" effect, which can be associated to a microscopic parameter, i.e., a "non-ideal parameter", hereafter. Because of it, magnetic reconnection makes a new dynamics accessible to the fluid plasma. Spontaneous magnetic reconnection usually occurs as an unstable process. In this framework, linear magnetic reconnection instabilities exist, which were first identified[5] in a tokamak geometry and go under the name of "tearing-type" modes. In a slab geometry, different wavelength regimes can be recognised. These can be mapped into the different tearing-type modes, which in a tokamak geometry correspond to distinct instabilities (see, e.g., Ref. 6).

Magnetic reconnection at the EMHD scales can spontaneously occur, for example, in solar wind turbulence (for a discussion of the relevance of EMHD reconnection to the more recent notion of "electron-only reconnection[7,8]" observed with in situ spacecraft measures, see Refs. 9). It can be also relevant to laboratory magnetized plasmas[10,11] in regimes where whistler waves[12–14] are the normal modes of the system −see Refs.15 and 16 for an overview of whistler wave phenomena in space and laboratory plasmas. Helicon devices are an example of these systems, as helicon waves in plasmas are essentially whistler waves propagating in a spatially bounded domain[17].

The EMHD modelling has been however adopted also for some regimes of description of tokamak physics[18] and for the confinement of an electron plasma in stellarators and toroidal trapping devices[19–21]. Besides of that, the experimental[7,8,22–25] and numerical[26–32] evidence that an electron dominated regime can be achieved *locally* in space and time intervals which are relatively narrow with respect to the bulk plasma dynamics but which are relevant to the electron dynamics, is strongly indicative that an EMHD-type modelling may be relevant also for the small-scale plasma dynamics of fusion devices and, generally speaking, of magnetically confined plasmas. In this sense, EMHD reconnection may be expected to occur[9] in a wide variety of magnetized plasmas, met both in space and laboratory.

In this work we extend the numerical analysis of linear

[a)]Electronic mail: homam.betar@univ-amu.fr
[b)]Electronic mail: daniele.del-sarto@univ-lorraine.fr
[c)]Electronic mail: alain.ghizzo@univ-lorraine.fr
[d)]Electronic mail: frederic.brochard@univ-lorraine.fr
[e)]Electronic mail: david.zarzoso-fernandez@univ-amu.fr

EMHD tearing-type modes to multi-parameter regimes of possible experimental relevance to laboratory plasmas and to solar wind turbulence. To this purpose, we perform a numerical study in which two or more non-ideal effects are retained at the same time. In these regimes there are not any analytical estimates presently available for the scaling laws of the characteristic scales associated to the eigenmodes. The results we obtain are interpreted by comparison with those of the single-parameter studies already known from literature and recently revised/complemented in Ref. 9. New, non-trivial regimes are thus identified, especially in the presence of electron viscosity, in which the asymptotic scalings of the growth rates and of the characteristic scale lengths associated to the eigenfunction depart from the usual power-law dependence which is typically met in other tearing regimes. These non-trivial regimes are determined by the competition between electron inertia and resistivity, whose effects in the EMHD regime can "overlap" in a wider parameter space interval than what is met, for example, in reduced MHD (cf. Ref. 33), or they are determined by the further inclusion of a finite viscosity. For example, when the contribution of the viscosity parallel to the guide field combines with electron inertia or with resistivity, an inversion of the sign of some power law scaling is found in a finite interval of the parameter space (the consistency of which we discuss, later).

Due to the complex behaviour which characterizes these reconnection regimes and due to the lack of theoretical works providing reference analytical estimates, we have however preferred to perform here a quantitative study by focusing on the general behaviour of the eigenmodes on the non-ideal parameters at play, without pretending to provide the "exact" power law scalings (also consider that −as we will see− a local approximation with a power law dependence seems to be feasible only in limited intervals of the parameter space). Quantitative estimates of the power-law scalings will be provided only in some reconnection regimes, in order to make comparison with known one-parameter limits or with some heuristic-type arguments. However, these estimates should be read as generally indicative: the problem of ascertain the "exact" power-law scalings from numerical fits in these reconnection regimes has been already extensively discussed in Ref. 9, where it has been pointed out how combining *both* an accurate numerical investigation over a wide parameter interval *and* some heuristic arguments providing consistency constraints may be necessary, in order to discern between rational exponents which differ one each other by just some decimal digits. A study of that kind goes beyond the purpose of the present work, which has the following structure.

In Sec. II the general features of the model are recalled. The limitations of the simplifying assumptions of the incompressible EMHD for the modelling of plasmas of experimental interest are discussed in Sec. II A.

In Sec. III we discuss the definition and normalization of the non-ideal dimensionless parameters of the problem (subsection III A) and their relevance to plasmas of experimental interest, both in laboratory and in astrophysics (subsection III B). The difference between the resistive and viscous coefficients parallel and perpendicular to the guide magnetic filed are therein discussed. The physical and dimensionless parameters of interest to a number of real cases are listed in Tables I and II.

Sec. IV is devoted to recall the general features of the linear problem. Here we introduce the definition of the characteristic spatial and time scales associated to the gradients of the eigenfunction, and we discuss some features of the procedural methods we are going to apply.

Sec. V concerns the numerical studies related to a two-parameter dependence: the regime where only electron inertia and an isotropic resistivity are retained (subsection V A); the regime where electron inertia and a perpendicular viscosity or where an isotropic resistivity and a perpendicular viscosity are retained (subsection V B); the regime where only a parallel and perpendicular viscosity are independently and simultaneously considered (subsection V C); the regime where electron inertia and a parallel viscosity or where an isotropic resistivity and a parallel viscosity are retained (subsection V D).

Sec. VI concerns the cases in which more than two non-ideal parameters at a time are simultaneously retained. In subsection VI A regimes of practical interest are considered, where a finite electron inertia combines with an isotropic resistivity and an isotropic viscosity. In subsection VI B a more realistic case in which electron inertia combines with a slightly anisotropic resistivity and with a highly anisotropic viscosity is studied, under the assumption that the resistivity and the parallel viscosity are comparable in magnitude and are much larger than the perpendicular viscosity.

In Sec. VII conclusions are drawn.

II. INCOMPRESSIBLE EMHD MODEL

We consider here the incompressible EMHD model discussed for example by Kingsep et al[1] and by Gordeev et al[2]. In this non-relativistic fluid model ions constitute a neutralizing immobile background and the electron fluid is assumed to be incompressible. In a 2D slab geometry, the relevant fluid equations ruling the nonlinear dynamics of tearing-type modes can be cast in the following form:

$$\frac{\partial}{\partial t}(\psi - d_e^2\nabla^2\psi) + [b, \psi - d_e^2\nabla^2\psi] = R_\perp\nabla^2\psi - V_\perp\nabla^4\psi \quad (1)$$

$$\frac{\partial}{\partial t}(b - d_e^2\nabla^2 b) + [b, b - d_e^2\nabla^2 b] = [\nabla^2\psi, \psi] + R_{||}\nabla^2 b - V_{||}\nabla^4 b. \quad (2)$$

where the magnetic field is given by $\mathbf{B} = \nabla\psi(x,y,t)\times\mathbf{e}_z + (B_0 + b(x,y,t))\mathbf{e}_z$, with B_0 representing the guide field. In this model we have included also dissipation effects, related to the non-ideal dimensionless parameters appearing above as diffusion-like coefficients $R_\perp$, $R_{||}$, $V_\perp$ and $V_{||}$, labeled with respect to the guide field orientation (for a more detailed derivation of the model, see, e.g., Ref. 9 and references therein); the normalized electron skin depth $d_e = \bar{d}_e/L_0$, where L_0 is a reference length and $\bar{d}_e = c/\omega_{pe}$ is the electron skin depth (c being the light speed and ω_{pe} the plasma frequency) is instead

related to the electron inertia. These parameters are discussed in greater detail in Section III B, next.

Combining Eqs. (1-2) −namely, adding twice Eq.(1), once multiplied by ψ and once multiplied by $\nabla^2\psi$, respectively, to Eq.(2) multiplied by b, and integrating by part over the whole plasma volume− we obtain the following energy equation:

$$\int \frac{1}{2}\frac{\partial}{\partial t}\left\{|b|^2+d_e^2|\nabla b|^2+|\nabla\psi|^2+d_e^2|\nabla^2\psi|^2\right\}dxdy = -\int\left\{R_\perp|\nabla\psi|^2+R_{||}|\nabla b|^2+V_\perp|\nabla^3\psi|^2+V_{||}|\nabla^3 b|^2\right\}dxdy. \quad (3)$$

The normalized terms in Eq. (3) can be interpreted, respectively, as: the magnetic energy density associated to the z- and (x,y) components, i.e., $B_z^2/(2\mu_0) \leftrightarrow |b|^2$ and $|\boldsymbol{B}_\perp|^2/(2\mu_0) \leftrightarrow |\boldsymbol{\nabla}\psi|^2$; the kinetic energy density along z and in the (x,y) plane, i.e., $m_e n_e u_{e,z}^2/2 \leftrightarrow d_e^2|\boldsymbol{\nabla}\psi|^2$ and $m_e n_e|\boldsymbol{u}_{e,\perp}^2/2 \leftrightarrow d_e^2|\boldsymbol{\nabla} b|^2$; the energy densities dissipated by the parallel and perpendicular resistivity (i.e., electron-ion viscosity), $R_{||}|\boldsymbol{\nabla} b|^2$ and $R_\perp|\boldsymbol{\nabla}\psi|^2$; the energy densities dissipated by the parallel and perpendicular viscosity (i.e., electron-electron viscosity), $V_{||}|\nabla^3 b|^2 = V_{||}|\boldsymbol{\nabla}\nabla^2 b|^2$ and $V_\perp|\boldsymbol{\nabla}^3\psi|^2 = V_\perp|\boldsymbol{\nabla}\nabla^2\psi|^2$.

A. Limitations and relevance of the incompressible EMHD model in laboratory and in astrophysics

As discussed in Ref. 9, the incompressible EMHD model of Eqs. (1-2) can be assumed to provide an incompressible fluid plasma description restricted to the electron dynamics −i.e., an "electron-only" dynamics, as it has been dubbed in recent literature[8]−, which is valid *locally* with respect to temporal and spatial scales at which the ion dynamics is negligible. In this sense, the validity of this EMHD model can in principle extend beyond the limits set in terms[1,2] of the global conditions for the propagation of EMHD linear modes, when $kd_i \lesssim 1$ and $\Omega_i \ll \omega \lesssim \Omega_e$. As discussed in the aforementioned work, there is indeed enough evidence from both spacecraft measurements[7,8,22–25], kinetic numerical simulations[27? ? –31] and theoretical models[27,32,34] that this can be the case. Interestingly, this ensemble of works suggests that the EMHD regime may be locally attained under conditions that can considerably differ from one another. For example, in the case of solar wind turbulence, an electron-only reconnection is observed in correspondence to small-scale turbulence, when at large scales the ion and electron temperature are comparable, $T_i \simeq T_e$. This condition can be more conveniently expressed in terms of the β-parameter of each species. For the typical solar wind turbulence this condition reads $\beta_i \simeq \beta_e \simeq 1$, where $\beta_\alpha = 2\mu_0(n_0 k_B T_\alpha)/B_0^2$. The theoretical reduction techniques based on a gyrokinetic[27,34] or on a gyrofluid[32] model, require instead that $\beta_e \ll 1$. Then, depending on the theoretical model, different orderings in terms of the electron-to-ion mass ratio $\varepsilon_m \equiv m_e/m_i$ can be formally required: for example, $\beta_i \sim \beta_e \sim \varepsilon_m \ll 1$ is required in Ref. 27 and 34, whereas $\beta_e \sim \varepsilon_m$ and $\beta_i \simeq 1/\varepsilon_m \gg 1$ is required in Ref. 32. Note that this latter result agrees with the remarks already provided in Ref. 27, in which Mallet argued (see therein) that the condition $\beta_i \ll 1$ imposed by the gyrokinetic derivation were probably too restrictive.

While, on the one hand, all this leaves open to future investigation the problem of better determining when a regime dominated by the electron dynamics can be locally attained, on the other hand it points to the possible relevance of EMHD to diverse contexts of plasma physics, which go beyond applications to space plasmas. The relevance to experimental measures of the simplified EMHD model we have considered is therefore subject to two main types of constraints: (i) the local negligibility of ion dynamics and (ii) the appropriateness of an incompressible closure for the electron fluid. Let us address these points separately.

Space plasmas like the solar wind are the most natural frameworks where hypotheses (i) and (ii) are more easily verified. For example, by referring to the data reported in Ref. 8 for an electron-only physics case (hp (i) satisfied) we can estimate $\Omega_{ce}/\omega_{pe} = 0.027$. Following Ref.[35] by ordering small density fluctuations as $\delta n_e/n_o \sim (\Omega_{ce}/\omega_{pe})^2 \simeq 7\times10^{-4}$ we can thus estimate that density fluctuations are negligible.

1. *Potential relevance of the EMHD regime to magnetically confined plasmas*

Historically speaking, the incompressible EMHD model has been first devised with application to magnetically confinement devices[10,11,17]. In particular, since it provides a natural framework for the description of whistler waves (see, e.g. Ref. 15), which in a bounded domain are also called "helicons", EMHD is particularly relevant to describe the electron physics in the so-called helicon devices[17,36]. In particular, incompressible EMHD has been used[37] to model magnetic reconnection (in the collisionless limit) in machines like the VINETA-II[38].

Less evident can be the relevance of the EMHD model to devices specifically designed to achieve thermonuclear fusion conditions. The study of plasma physics in these systems is indeed generally oriented, from both an experimental and a theoretical point of view, to the investigation of the physics at the ion scales, which dominate the bulk plasma dynamics. EMHD has been however adopted to provide a fluid model of the current dynamics in stellarators and toroidal fusion devices[18,21]. Moreover, the detection of a whistler dynamics[39–41] is a signature of the general relevance of the EMHD regime for fusion plasmas −albeit, of course, the restriction to the incompressible limit may here be a too crude approximation. In general, indeed, the inclusion of kinetic effects may be required, especially because of the high temperature attained by electrons in these conditions; comparable electron temperatures (i.e., $T_e \gtrsim 5\,keV$) have been locally measured also in magnetospheric plasmas where whistler waves have been detected[42]. There is nowadays recognised evidence that, in tokamak plasmas, the whistler dynamics is associated for example to the excitation of runaway electrons (see, e.g., Refs. 41, 43, and 44, just to cite a few). Although runaways electrons can attain relativistic velocities (see, e.g., Refs. 45–47) and are likely

to be dominated by kinetic effects, they provide a quite fitting example of current jets in which ion physics is negligible. Incompressible EMHD models have been thus also used to describe some features of their physics[48–50]. In this light, the incompressible EMHD model we adopt here, can be seen as a first attempt to investigate electron-only tearing-type instabilities which can be possibly associated to the dynamics of intense currents nonlinearly generated in tokamaks, although no evidence of these phenomena has been reported so far: in this sense, the parameters of machines like ITER and JET reported in Tables I and II, next, are reported just as a term of comparison and their relevance to EMHD tearing modes must be regarded as purely speculative.

2. *Limitations of the incompressible limit*

The incompressibility of the electron fluid is not appropriate when charge separation effects are important. The evolution of the charge density is naturally associated to relativistic effects, the time derivative of the charge density in the corresponding continuity equation being related to the displacement current in Ampére's law. As we have seen, however, relativistic effects can be important in the EMHD regime.

In Refs. 35 charge separation and relativistic effects have been accounted for as first order density perturbations ordered like $\delta n_e/n_0 \sim (\Omega_{ce}^2/\omega_{pe}^2) \ll 1$, which were shown to be related to the diffusion of the small perturbations of the parallel component of the magnetic field. Once included in the study of tearing modes[3,51,52] these corrections just enter with a "renormalization" of the electron skin depth, which gets a small additive term becoming $\lambda_e^2 = d_e^2(1+\Omega_{ce}^2/\omega_{pe}^2)$.

Other works[53–56], even prior to Ref. 35, have included electron compressibility related to slow density variations resulting from the nonlinearities associated with the whistler wave dynamics[56] in a non-perturbative way. These effects, generate electric fields responsible for the ion response occurring on the same timescales characterizing the evolution of these electric fields. These effects can have important consequences for the energy cascade in electron whistler turbulence[57] and in the decay of whistlers and helicons involving low frequency, slow waves (see, e.g., Refs. 58–60).

The fluid electron incompressibility also excludes from the model any electron temperature effect, even when non-isothermal, polytropic closures are considered. This is another limitation of the model, which has been overcome in some works like Refs.[54,55,61]. Therein an equation describing the evolution of electron temperature, no longer considered constant, has been included.

Despite all these effects may be important in the EMHD parameter range we consider, here we neglect them as a first approximation, the purpose of the present work being to focus on the tearing mode analysis, as it was laid down in the seminal work by Furth et al.[5], in which electrostatic and non-isothermal effects were all neglected. The aim of this work is indeed to provide a first assessment of the combined role of two or more non-ideal parameters, once accounted for simoultaneously (in previous literature, they have been mostly considered separately in the EMHD regime). As discussed in Ref. 9, this approach is meant as a first step towards the extension of the linear tearing mode analysis in kinetic EMHD regimes.

III. NON-IDEAL EMHD PARAMETERS AND RECONNECTION REGIMES OF EXPERIMENTAL INTEREST

A. Non-ideal parameters and their normalization

In Eqs.(1-2) the lengths are normalized to a reference length L_0 and times to a characteristic whistler time τ_w, which corresponds to the propagation of whistler waves along the guide magnetic field over a distance L_0. For the moment we can define it as $\tau_w \equiv n_e e L_0^2/(\varepsilon_0 B_0 c^2)$ in terms of the physical parameters, among which we have introduced the density (n_e) and charge ($-e$) of the electrons, and the vacuum permittivity (ε_0). This time-scale naturally appears in the $\bar{k}_{||}L_0 \to 1$ and $\bar{d}_e^2/L_0^2 = d_e^2 \ll 1$ limits of the dispersion relation of whistler waves,

$$\omega = \Omega_{ce}\bar{d}_e^2 \frac{\bar{k}\bar{k}_{||}}{1+k^2\bar{d}_e^2}, \qquad \Omega_{ce} \equiv \frac{eB_0}{m_e}, \tag{4}$$

where $\bar{k}$ and $\bar{k}_{||}$ respectively denote the amplitude of the dimensional wave-vector and of its component along the guide field, and Ω_{ce} is the electron cyclotron frequency. Eq.(4) is straightforwardly obtained by linearizing the system (1-2) in the $R_\perp = R_{||} = V_\perp = V_{||} = 0$ limit around a uniform magnetic field $\boldsymbol{B}_0$ −for example, aligned with y, and for a perturbation with $\bar{\boldsymbol{k}} = \bar{k}_\perp \boldsymbol{e}_x + \bar{k}_{||}\boldsymbol{e}_y$ and $\bar{k} = (\bar{k}_\perp^2 + \bar{k}_{||}^2)^{1/2}$. Then

$$\tau_w = \frac{L_0^2}{\bar{d}_e^2 \Omega_{ce}} \tag{5}$$

The diffusion-like coefficients appearing at r.h.s. of Eqs. (1-2) can be defined by introducing some characteristic diffusion times in the directions perpendicular and parallel to the guide field. In the case of the R-coefficients, we introduce the diffusion times

$$\tau_\perp = \frac{\mu_0 L_0^2}{\eta_{e,\perp}}, \quad \tau_{||} = \frac{\mu_0 L_0^2}{\eta_{e,||}} \tag{6}$$

which are related to the resistive diffusion of the magnetic lines, and because of this are dependent on the resistivity coefficients $\eta_{e,\perp}$ and $\eta_{e,||}$ (cf. Eq.(32) in Ref. 9). Thus, we define the inverse perpendicular and parallel electron Lundquist numbers as follows:

$$R_\perp = \frac{\tau_w}{\tau_\perp}, \quad R_{||} = \frac{\tau_w}{\tau_{||}}. \tag{7}$$

For the V-coefficients we introduce the viscous diffusion

times

$$\hat{\tau}_\perp = \frac{L_0^4}{d_e^2 \mu_\perp}, \;\; \hat{\tau}_{||} = \frac{L_0^4}{d_e^2 \mu_{||}}, \tag{8}$$

dependent on the respective viscous coefficients $\mu_\perp$ and $\mu_{||}$, so to define the electron viscosity and hyper-viscosity numbers

$$V_\perp = \frac{\tau_w}{\hat{\tau}_\perp}, \;\; V_{||} = \frac{\tau_w}{\hat{\tau}_{||}}. \tag{9}$$

EMHD, as it is usually formulated in the sense of Refs.[1,2], is formally valid at time scales larger than or at most comparable to the electron cyclotron time, but much shorter than the ion cyclotron time. It also requires the characteristic lengths to be shorter than the ion skin depth $\bar{d}_i = \sqrt{m_i/m_e}(\bar{d}_e/Z)$ (which for an ion species of charge Z can be defined as $\bar{d}_i = \sqrt{m_i/m_e}(\bar{d}_e/Z)$). Because of this, the thickness the thickness of the current sheet possibly unstable to EMHD tearing modes must be not larger than $\bar{d}_i$.

Therefore

$$L_0 = a \sim s\bar{d}_i, \qquad s \leq 1, \tag{10}$$

is a reasonable choice for the reference length. Henceforth, for experimental application, we will take in particular the upper limit $s = 1$.

B. Some parameter range of possible experimental relevance

The linear problem we are going to study formally depends on the five parameters d_e, $R_\perp$, $R_{||}$, $V_\perp$, and $V_{||}$. However, looking at the dependence of each of these dimensionless parameters on the physical parameters of the plasma (in this case, the characteristic amplitude of the equilibrium magnetic field, B_0; the electron temperature T_e and particle density n_e; and the ion charge Z) can help us to narrow down their range of variability in reconnection regimes which are of practical relevance.

This is the rationale with which Table I has been constructed. Then, the physical parameters therein have been used, combined with the definitions of the dimensionless parameters (7-9) given in terms of the dimensional quantities, which were already discussed in Ref. 9, in order to compute the values in Table II. The numerical formulae we have used are those which follow, where all quantities are meant to be expressed in MKS units, except for energy, which is expressed in keV:

$$\bar{d}_e^2 = \frac{2.824 \times 10^{13}}{n_e a^2}, \qquad \bar{d}_i^2 = \frac{1}{Z^{*2}} \frac{m_i}{m_e} \bar{d}_e^2, \tag{11}$$

$$\begin{pmatrix} R_\perp \\ R_{||} \end{pmatrix} = \begin{pmatrix} 1.06 \\ 0.541 \end{pmatrix} \times 10^{-51} \times \frac{Z^* n_e \ln(\Lambda_e)}{B_0 T_e^{3/2}}, \tag{12}$$

$$\begin{pmatrix} V_\perp \\ V_{||} \end{pmatrix} = \begin{pmatrix} 1.74 \times 10^{-74} \dfrac{Z n_e^2 \ln(\Lambda_e)}{B_0^3 T_e^{1/2} a^2} \\ 1.55 \times 10^{+28} \dfrac{T_e^{5/2}}{Z B_0 \ln(\Lambda_e) a^2} \end{pmatrix}. \tag{13}$$

where n_e, B_0, and T_e are given in m^{-3}, Tesla, and keV units, respectively. Here Z^* is the effective atomic number reflecting the degree of ionization of each atom: one usually means a plasma to be "fully ionized" in the sense that the number of neutrals is negligible, but this does not mean that ions themselves are fully ionized, too, that is, in general $Z^* < Z$. In reality, indeed, $Z^* \leq 3$ in most laboratory devices. Notice in this regard that in any atom the ratio between the number of neutrons and that of protons in the nucleus is about unity for $Z < 20$ and it does not trespass ~ 1.6 for larger values of Z. It thus follows that $m_i < 2Zm_H$, for m_H representing the mass of the Hydrogen nucleus. As a consequence, the ratio d_i/d_e in a plasma with *each* atom which is fully ionized scales roughly as $1/Z$, meaning that the scale separation between d_i and d_e becomes narrower, for heavier fully ionized atoms. Instead, for a plasma with heavier atoms but with $Z^* \ll Z$, the scale separation between d_i and d_e increases with respect to the Hydrogen case with the square root of the ion mass species. This is the case of the Argon plasma in the laboratory devices displayed in Tables I-II, for which $Z^* \sim 1$ or 2 (throughout the table, the arbitrary value $Z^* = 1$ has been taken). We also note that, typically, plasmas of the laboratory devices of Tables I-II are not even fully ionized, and they may be constituted by a percentage of neutrals which can be well of the order of 10% of the total heavy species density. This fact is not expected to play a role in the EMHD reconnection regimes treated in this work, since neutrals are not going to appreciably affect the electron dynamics (they do not intervene in the charge balance and negligibly affect the electron collision rates), while their dynamics is completely neglected, so as that of ions is.

It is also interesting to note that, despite all coefficients of Eqs.(12-13) are related to collisions, they differently depend on the electron collision time which scales like $\tau_e \sim T_e^{3/2}/(\ln(\Lambda) Z n_e)$ –cf. Sec. V of Ref. 9.

Table II presents quantitative estimates for different non-ideal parameters in some magnetic confinement devices and for specific turbulent regimes of the solar wind. Non-helicon devices specifically dedicated to thermonuclear fusion experiments (ITER, JET) or magnetic reconnectiom studies (MRX, RFX) have been included for comparison and by following the rationale that an "electron-only" dynamics may be locally achieved, locally in space and time[9], as indicated by a number of studies focusing on plasma turbulence (cf. the discussion in Sec. I and Refs. 7, 8, 22–32).

In Table II, the dimensionless electron skin depth is defined as $d_e = \bar{d}_e/a$, where $\bar{d}_e$ represents its dimensional value. Additionally, these values have been calculated under the assumption that $L_0 = a = \bar{d}_i = \sqrt{m_i/(Z^2 m_e)}\bar{d}_e$.

According to the definition of the parallel and perpendicular resistivity and viscosity coefficients (cf. Ref. 62 and 63

and the discussion in Ref. 9), the following orderings can be established:

$$\frac{R_\perp}{R_{||}} = \frac{\eta_\perp}{\eta_{||}} \approx O(1) \qquad \frac{V_\perp}{V_{||}} = \frac{\mu_\perp}{\mu_{||}} \approx \frac{1}{\Omega_{ce}^2 \tau_e^2}, \tag{14}$$

where

$$\tau_e = \frac{6\sqrt{2}\pi^{\frac{3}{2}}\varepsilon_0^2\sqrt{m_e}T_e^{\frac{3}{2}}}{Z\ln\Lambda e^4 n_e} \tag{15}$$

is the characteristic time required for electrons to thermalize (i.e., it is the "electron collision time"). In its definition, $\ln\Lambda$ is the Coulomb logarithm, whose weak dependence on Z, T_e, and n_e makes it generally contribute with a numerical factor, which for practically all relevant application is comprised in the interval $10 \lesssim \ln\Lambda \lesssim 20$.

Since the model we rely upon requires that $\Omega_{ce}\tau_e \gg 1$, which is quite well verified for all cases considered in Tables I-II, Eqs. (14) generally imply that $V_\perp \ll V_{||}$. At the same time, however, the dependence of the ratio $V_\perp/V_{||}$ on many physical parameters allows for a quite large variability of the value of this ratio. Looking at the values in Table II one notes that $V_\perp/V_{||}$ in magnetically confined plasmas ranges from $\sim 10^{-19}$ to $\sim 10^{-6}$ and in the solar plasma ranges from $\sim 10^{-20}$ to $\sim 10^{-16}$..

IV. LINEAR ANALYSIS WITH A TWO- AND THREE-PARAMETER DEPENDENCE

We now focus on the linear study of tearing modes, performed by linearising Eqs.(1-2) around an equilibrium with[64] $\psi_0(x) = 1/(2\cosh^2(x))^{-1}$ and $b_0 = 0$ for modes of the kind $\sim f(x)\cos(ky)e^{\gamma t}$, and by solving numerically the corresponding eigenvalue problem with the solver detailed for reduced-MHD tearing modes in Ref. 33, and adapted for EMHD tearing regimes in Ref. 9. Like in the aforementioned works, we consider here three distinct wavelength regimes which are identifiable in a slab tearing geometry, and where power-law scalings of both the growth rate γ and of other microscopic scale lengths associated to the gradients of the eigenfunctions (see Ref. 6) are usually expected. Introducing the well-known instability parameter[5] $\Delta'(k)$ and the reconnection layer width δ (which can be operationally defined in terms of the gradient of the perturbed current function as proposed in Ref. 6), these three wavelength regimes can be respectively identified as: the large-Δ' limit, corresponding to $\Delta'\delta > 1$ (hereafter labelled with the index "LD"); the small-Δ' limit, corresponding to $\Delta'\delta < 1$ (hereafter labeled with the index "SD"); and the fastest growing mode limit (hereafter labelled with the index "M"), corresponding to the condition $\Delta'\delta \sim 1$. We recall that the instability condition $\Delta'(k) > 0$ fixes a range of unstable wavevectors in an interval $(0, k_m)$, where $k_m = \sqrt{5}$ for the equilibrium chosen here. Because of this, a correspondence of each of the three regimes expressed in terms of the value of Δ' with a wavelength range can be established: the LD limit corresponds to the $k \ll 1$ range; the SD limit corresponds to the $k \to k_m$ range; and the fastest mode limit corresponds to an asymptotic dependence of k on the powers of the non-ideal parameters, which can be deduced by singling out k as a function of the other parameters from the condition $\delta_{LD} \sim \delta_{SD}$, or from $\gamma_{LD} \sim \gamma_{SD}$, when it is not trivial (see Ref. 9 and 65). The other quantities, the asymptotic scaling of which we may be interested to evaluate, in the following, are the inverse scale lengths which in Ref. 6 have been introduced as

$$D' \equiv \lim_{\varepsilon\to 0} \frac{\psi_1'(+\varepsilon) - \psi_1'(-\varepsilon)}{\psi_1(0)}, \tag{16}$$
$$\Delta'_{v_y} \equiv \frac{v_{y,1}(\delta) - v_{y,1}(-\delta)}{v_{y,1}(\delta)} = \frac{2b_1''(\delta)}{b_1'(\delta)},$$

where the index "1" labels the perturbed quantities and $v_{y,1} = b_1'$ stands for the electron fluid velocity component along y. In the first of the equations (16) above, D' can be seen as a "generalisation" of the Δ' parameter first introduced in Ref. 5, and to which D' converges in the small-Δ' limit only (we recall that the definition of Δ' is similar to the first of Eqs. (16), provided ψ_1 is substituted with the part of the eigenfunction ψ_1 which solves the linear version of $[\psi, \nabla^2\psi] = 0$). In Ref. 6, in particular, it has been numerically verified that Δ' can be computed using the ratio at r.h.s. of the first of Eqs. (16), evaluated by removing the $\lim_{\varepsilon\to 0}$ and by substituting ε with δ. The quantity Δ'_v of the second of Eqs. (16) can be thus mimics the definition of Δ', once evaluated for the quantity b', corresponding to the electron velocity component along the neutral line. Both D' and Δ'_v have been shown to display non-trivial power-law scalings in different tearing regimes, both in reduced-MHD[6] and in EMHD[9]. In Ref.9, in particular, it was shown that in all wavelength limits $\Delta'_v \sim \delta^{-1}$, and that both D' and Δ'_v play an important role in the heuristic interpretation of the numerical results of the one-parameter eigenvalue problem, which is, in turn, important for the numerical estimate of power law scalings which respect some inner coherence. It should be noted that it is computationally quite demanding in some regimes to determine the scalings of the different quantities with respect to k. This generally happens in fastest mode limit, or when one tries to determine the scaling with respect to Δ' and to k in the small-Δ' limit with small non-ideal parameters, and/or when k approaches the marginally stable value k_m). In this case, the multi-precision version of the code, discussed in Ref.33, must be used, which considerably increases the computation time required to grant convergence of the numerical scheme. Because of this reason, and since in the following we are going to show that the asymptotic scalings of the quantities of interest do not respect anymore a power-law dependence on the non-ideal parameters, in the following we are going to omit to perform a specific study of the dependence of quantities on k, since our purpose, here, is mainly to evaluate the behaviour of the normal mode solutions with respect to the non-ideal parameters at play, when two or more of them are simultaneously taken into account.

An important element distinguishes however the present numerical approach to that of Ref.9, where the focus was primarily on conducting a single-parameter study of different tearing regimes. Here, instead, since the variability of

the parameters in the Table II underscores the importance of considering more complex, multi-parameter regimes in realistic scenarios, we extend that analysis to two-parameter and to three-parameter regimes. For example, while we can still keep on assuming, like in Ref.9, a proportionality between $R_\perp$ and $R_{||}$, since the ratio $R_{||}/R_\perp$ is only weakly dependent[62] on Z (i.e., $R_\perp/R_{||} \simeq 3$ for $Z \Longrightarrow \infty$ and $R_\perp/R_{||} \simeq 2$ for $Z = 1$), the proportionality between $V_\perp$ and $V_{||}$ already considered in previous studies[9,66] will be relaxed, in the following.

Due to the general, relative smallness of the estimated values of $V_\perp$ and $V_{||}$ with respect to both d_e and $R_\perp$, $R_{||}$, which are reported in Table II, it may seem a priori quite reasonable to neglect as a first approximation the electron viscosity. As we will see in the following, however, several order of magnitudes separating the viscosity coefficients from the normalized electron inertia or the resistivity do not generally grant the negligibility of $V_\perp$ and in particular $V_{||}$, which, instead, may radically modify the scaling laws with respect to the other parameters, as well. This is one of the results of the present analysis, which we will discuss later. This dependence can be qualitatively understood by considering the high order of the spatial derivative weighted by the $V_\perp$ and $V_{||}$ coefficients, which make them more important, the smaller the characteristic width of the reconnecting layer is. The latter, is in turn generally thinner, the smaller d_e and $R_\perp$, $R_{||}$ are. At the same time, it should be noted that accounting for numerical values of the viscosity, which adhere to the estimates of Table II, is extremely costly from the computational point of view. This is why, in the preliminary multi-parameter study of EMHD tearing modes that follows, we have opted for investigating regimes in which the scale separation between the non-ideal parameters considered may be significant and can follow the trends suggested by the values in Table II, although the ranges of values of the viscosity (and $V_\perp$, in particular), may be significantly different from those reported therein.

Finally, it is worth underlining a point of the following discussion, which is important from the methodological point of view. The regimes we are going to discuss, next, seem to have been not investigated, yet, in previous literature, neither from an analytical nor from a numerical point of view (if not for few cases). Therefore, the scalings we have obtained lack of terms of comparison. Moreover, in many cases of multi-parameter dependence, we are going to show that these scalings depart, in significant intervals of the parameter space, from the "usual" power-law dependencies known in other tearing reconnection regimes. Because of this, and considering the practical difficulty to identify the exponent of a power law scaling (e.g., distinguishing close fractional values from a numerical fit), which has been already pointed out in Ref. 9, whenever we are going to present some power law scaling not supported by theoretical estimates, next, it should be read just as an "indicative estimate". Nevertheless, some consistency argument in support of the numerical results obtained will be given. One is typically the verification of the convergence of the numerical results to the scaling of some known 1-parameter limit. Another argument, applicable only in the resistive and inertial regimes, concerns the formal equivalence of the two reconnection regimes, provided the correspondence $\gamma d_e^2 \leftrightarrow R$ (which is the EMHD version of the correspondence $\gamma d_e^2 \leftrightarrow S^{-1}$ of reduced MHD −see Refs. 6 and 67).

In general, whenever in the figures of this article some specific estimate of a power-law scaling is shown, the following convention is applied:

-) Solid black lines (and black printed scaling values) correspond to some indicative numerical fit, estimated to be valid in a parameter interval of the results. These scalings are, to the best of our knowledge, new.

-) Solid red lines (and red printed scaling values) correspond to power-law scalings of single parameter regimes, which have been already established in previous works and are here presented, typically for comparison.

-) Dashed black lines (and black printed scaling values) indicate arbitrary power-law scalings, shown in the figure as a term of comparison with respect to the actual parameter dependence of the displayed quantities.

V. TEARING MODES WITH A TWO-PARAMETERS DEPENDENCE

A. Dependence of γ on (d_e, R)

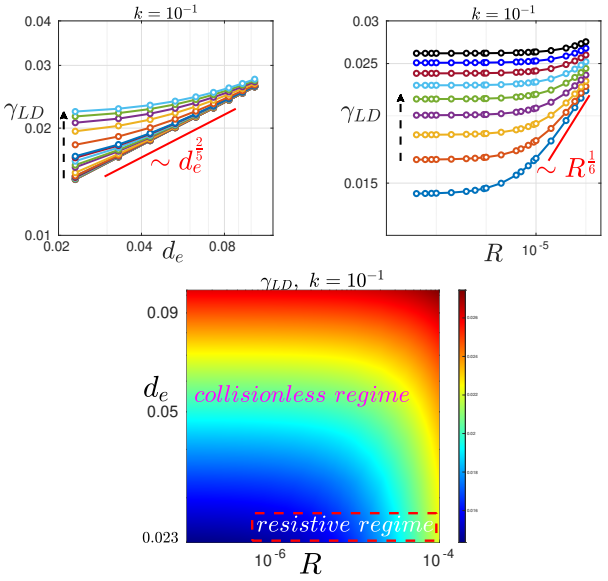

FIG. 1. Growth rate for the large-Δ' limit as function of d_e and R in the top-left and top-right frames, respectively. Top frames: the vertical dashed arrows show the direction in which the parameter R (left frame) or d_e (right frame) increases; the parameter intervals considered are $R \in [4\times10^{-8}, 8\times10^{-4}]$ (left frame) and $d_e \in [0.023, 0.103]$ (right frame). Bottom frame: 2D representation of the growth rate.

We start by investigating a scenario where both resistivity and electron inertia are retained in a parameter space relevant to various realistic regimes, while viscosity, as a first approximation, is neglected.

Since $R_\perp$ and $R_{||}$ always differ just by a numerical factor of order 2 or 3 (cf. Eq. (14)), and having already shown[9]

TABLE I. : The physical parameters of the table below have been taken from the references indicated in the first column. The first three lines correspond to theta pinch-type devices (LAPD, SPEKTRE, VINETA II). The fourth and fifth line correspond to tokamaks (ITER, under construction, and JET). The sixth and seventh line correspond to machines specifically designed for magnetic reconnection experiments (MRX and RSX). Then, for lines related to parameters of the Sun plasma are given, which refer to characteristic values met at different distances from the Sun center (these are indicated in the first column in Astronomical Units). The Coulomb logarithms for electron-electron collisions (last column) have been evaluated as[63] $\ln\Lambda \simeq 23.4 - 1.15\log n_e + 3.45\log T_e$, which is valid for $T_e < 50\,eV$, while for ITER and JET cases, where $T_e \gg 50\,eV$, the Coulomb logarithms read $\ln\Lambda \simeq 14.9 - 0.5\log n_e + \log T_e$ with n_e and T_e given in m^{-3} and keV, respectively. The value of τ_e has been evaluated using Eq. (15). All parameters are indicated in cgs units; eV is used for the energy.

Device	ions	m_i/m_e	$n_e[m^{-3}]$	$B_0[Tesla]$	$T_e[eV]$	$\ln\Lambda$	$\tau_e[sec]$	$\Omega_e[sec^{-1}]$
LAPD[68]	H – He	1836 – 7344	$10^{17} - 10^{19}$	$(4-35)\times 10^{-2}$	$1-12$	$8-14$	$(2-5000)\times 10^{-8}$	$(7-62)\times 10^{9}$
SPEKTRE[69]	H-He	1836 – 7344	$10^{16} - 10^{19}$	$(5-44)\times 10^{-2}$	$3-10$	$10-15$	$(8-4000)\times 10^{-8}$	$(9-80)\times 10^{9}$
VINETA II[38]	Ar	73440	$10^{16} - 10^{20}$	$0.1-0.16$	$5-10$	$9-15$	$(2-40000)\times 10^{-8}$	$(2-3)\times 10^{10}$
ITER[70]	D-T	3672 – 5508	10^{20}	5.3	$(1-1.5)\times 10^{4}$	$21-22$	$(1-2)\times 10^{-3}$	9×10^{11}
JET[71]	D-T	3672 – 5508	$10^{19} - 10^{20}$	$2-3.5$	$(2-6)\times 10^{3}$	$22-25$	$(1-50)\times 10^{-4}$	$(4-6)\times 10^{11}$
MRX[72]	H-He	1836 – 7344	$10^{19} - 10^{20}$	$0.02-0.1$	$5-15$	$10-13$	$(2-80)\times 10^{-8}$	$(4-20)\times 10^{9}$
RSX[73]	H	1836	$(1-3)\times 10^{19}$	$0.01-0.04$	$6-14$	$10-12$	$(7-70)\times 10^{-8}$	$(2-7)\times 10^{9}$
Solar plasma (ideal distance from Sun's center)								
$0.0046\,AU = 1\ R_\odot$ (photosphere)[74,75]	H	1836	10^{10}	$(5-50)\times 10^{-3}$	0.6	18	5.5	$(9-90)\times 10^{8}$
0.0052 AU (upper corona)[76]	H	1836	10^{12}	10^{-4}	86	18	87	2×10^{7}
0.17 AU ($\simeq 35.7\,R_\odot$)[77,78]	H	1836	3×10^{8}	1×10^{-8}	30	25	5.8×10^{4}	1.7×10^{3}
1 AU (solar wind)[76]	H	1836	3×10^{6}	3×10^{-9}	8.6	26	9×10^{5}	5.3×10^{2}

TABLE II. : : The dimensionless parameters of the table below have been computed using formulae (11 -15) specialized for $Z^* = 1$ and for the values of the physical parameters listed in Table II. The product $\Omega_e \tau_e$ in the first column is indicative of the applicability of Braginski-type estimates (in case it is much larger than unity): it has been evaluated (and rounded) combining the values of Table I (e.g., $\max\{T_e\}$ with $\min\{B_0\}$ and $\min\{n_e\}$) by following, for experimental devices, the rationale that the maximum (minimum) value of B_0 generally goes together with the maximum (minimum) value of n_e. The shear length a appearing in the fourth column is left as a free parameter, to be expressed in *cm*.

	$\Omega_e \tau_e$	d_i^2/d_e^2	d_e	$R_\perp$	$R_\parallel$	$V_\perp$	$V_\parallel$
Device							
LAPD	$(1-370)\times 10^3$	1836– 7344	$\frac{(17-531)\times 10^{-4}}{a}$	$(3-1000)\times 10^{-6}$	$(1-500)\times 10^{-6}$	$(1-5000)\times 10^{-26}$	$(5-30000)\times 10^{-18}$
SPEKTRE	$(6-3000)\times 10^3$	1836 – 7344	$\frac{(17-531)\times 10^{-4}}{a}$	$(3-2000)\times 10^{-7}$	$(1-900)\times 10^{-7}$	$(6-10^7)\times 10^{-30}$	$(5-10^4)\times 10^{-18}$
VINETA II	$(25-130)\times 10^2$	73440	$\frac{(0.5-53)\times 10^{-3}}{a}$	$(1-20000)\times 10^{-7}$	$(7-2\times 10^{12})\times 10^{-31}$	$(7-2\times 10^5)\times 10^{-18}$	$(9-4\times 10^5)\times 10^{-18}$
ITER	$(1-2)\times 10^9$	3672 - 5508	$\frac{(5.3-17)\times 10^{-4}}{a}$	$(5-10)\times 10^{-10}$	$(3-5)\times 10^{-10}$	$(1-2)\times 10^{-25}$	$(3-7)\times 10^{-7}$
JET	$(6-200)\times 10^7$	3672-5508	$\frac{(5.3-17)\times 10^{-4}}{a}$	$(5-200)\times 10^{-10}$	$(3-80)\times 10^{-10}$	$(4-10^3)\times 10^{-27}$	$(1-100)\times 10^{-9}$
MRX	$(3-30)\times 10^2$	1836-7344	$\frac{(5.3-17)\times 10^{-4}}{a}$	$(4-30)\times 10^{-4}$	$(2-20)\times 10^{-4}$	$(7-90)\times 10^{-20}$	$(5-200)\times 10^{-14}$
RSX	$(4-20)\times 10^2$	1836	$\frac{(9-17)\times 10^{-4}}{a}$	$(6-30)\times 10^{-4}$	$(3-10)\times 10^{-4}$	$(2-8)\times 10^{-19}$	$(1-10)\times 10^{-13}$
Solar plasma							
0.0046AU	$(5-50)\times 10^{10}$	1836	$\frac{53}{a}$	$(2-20)\times 10^{-11}$	$(1-10)\times 10^{-11}$	$(3-3000)\times 10^{-47}$	$(9-90)\times 10^{-26}$
0.0052 AU	2×10^9	1836	$\frac{5.3}{a}$	7×10^{-10}	3×10^{-10}	3×10^{-34}	10^{-15}
0.17 AU	10^8	1836	$\frac{307}{a}$	10^{-8}	5×10^{-9}	10^{-32}	2×10^{-16}
1 AU	5×10^8	1836	$\frac{3070}{a}$	2×10^{-9}	10^{-9}	10^{-36}	3×10^{-19}

that a proportionality relation between $R_\perp$ and $R_{||}$ yields the same scaling law (except for multiplying numerical factors) of the $R_\perp = R_{||} = R$ case, we consider here a single, isotropic resistivity coefficient.

In all three wavelength limits considered, the same general behaviour has been identified, which is characterized by the existence of two opposite regimes: a purely resistive one, where R dominates and d_e is negligible, and a collisionless one, where d_e dominates, instead, and R is negligible. Similarly to what was noted[33] in reduced MHD, the transition between the collisionless and resistive regimes is characterized by a regime, narrower in the parameter space, where power-law scalings are no longer valid. This transition phase is relevant in certain realistic regimes. This may be the case, for example, of some operational regimes in both SPEKTRE and VINETA II (cf. Table II). Several previous studies[3,9,51,79–83] have already extensively explored electron-MHD tearing modes when resistivity and electron inertia are separately considered. In Fig.1 we thus present results only for the large-Δ' limit, with the purpose to highlight the transition between the purely resistive and the purely collisionless regime (the small-Δ' limit and the fastest mode limit exhibit a qualitatively analogous behavior).

In particular, the upper frames of Fig.1 show the scaling laws of the growth rate at fixed k as a function of d_e for various values of R (the top-left frame) and as a function of R for different values of d_e (top-right frame). The different curves of the top-left frame correspond to the values of the non-ideal parameter on the x-axis of the top-right frame, and vice-versa. The bottom frame of the same Figure shows $\gamma_{LD} = \gamma_{LD}(R, d_e)$ for a fixed value of k, chosen so that in the whole parameter space considered, the LD is recovered. Here, the resistive regime can be identified as the region of the parameter space roughly contained inside of the dashed red-colored rectangle. The power laws identified in both the collisionless and resistive limits, i.e., $\gamma_{LD} \sim d_e^{2/5}$ for $\gamma_{LD} d_e^2 \gg R$ and $\gamma_{LD} \sim R^{1/6}$ for $\gamma_{LD} d_e^2 \ll R$, respectively, and explicitly shown in the upper frames agree with those numerically identified in Ref. 9.

B. Dependence of γ on $(d_e, V_\perp)$ and on $(R, V_\perp)$

Here we focus on the general dependence of γ on the couples of parameters $(d_e, V_\perp)$ and $(R, V_\perp)$, separately considered. Although the parallel electron (hyper-)viscosity is often largely dominant over the perpendicular viscosity, we consider here the formal limit $V_{||} = 0$ as an example of a two-parameter dependence in which both parameters retained can separately induce reconnection and drive the tearing mode growth. Furthermore, exploring these regimes provides a possible benchmark test for when further non-ideal parameters are incorporated in the tearing mode analysis, or for nonlinear simulations, e.g. when hyper-viscosity is included.

Although not any other quantitative estimates are available for the scalings in these regimes, the numerical results shown below in the inertial ($d_e \neq 0$) and resistive ($R \neq 0$) regimes display an inner coherence, as they can be recovered one from the other by substituting γd_e^2 with R. This correspondence will be discussed below.

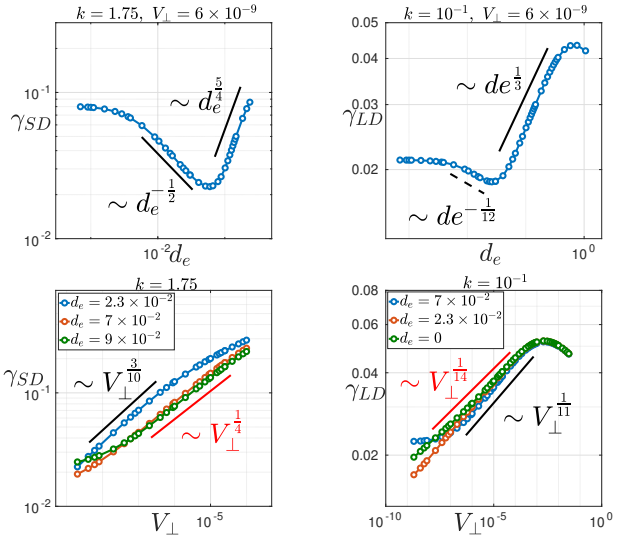

FIG. 2. Top frames: the scaling laws of the growth rate as a function of d_e for only one value of $V_\perp$. Bottom frames: the scaling laws of the growth rate as a function of $V_\perp$. Left frames correspond to the small-Δ' limit, while the right frames represent the large-Δ' limit in $(d_e, V_\perp)$. The parameter intervals considered are $d_e \in [0.023, 0.103]$ (top frames), $V_\perp \in [2 \times 10^{-9}, 10^{-5}]$ (bottom frames).

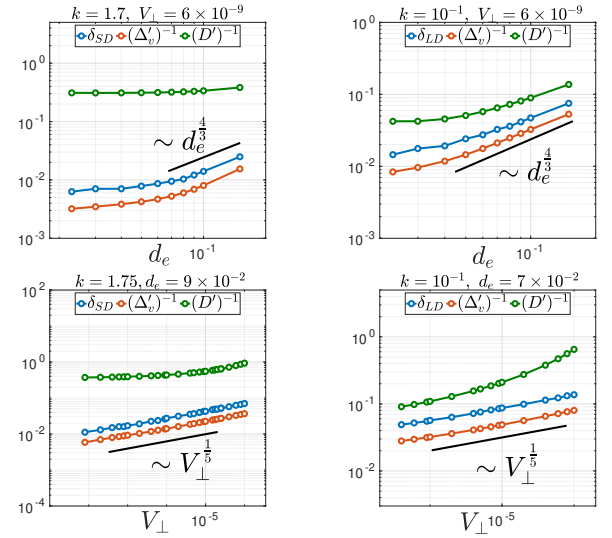

FIG. 3. Top frames: the scaling laws of the spatial scales as a function of d_e. Bottom frames: the scaling laws of spatial scales as a function of $V_\perp$. Left frames correspond to the small-Δ' limit, while the right frames represent the large-Δ' limit in $(d_e, V_\perp)$ regime. The parameter intervals considered are $d_e \in [0.023, 0.103]$ (top frames), $V_\perp \in [10^{-9}, 10^{-4}]$ (bottom frames.

Fig.2 and Fig.3 show the growth rate and the width of the reconnecting layer, respectively, both in the small (left frames) and large (right frames) Δ' limits of the $(d_e, V_\perp)$ regime.

This regime (and, subsequently, also the $(R, V_\perp)$ regime) is quite interesting from a theoretical point of view, since it shows that the two effects (electron inertia and perpendicu-

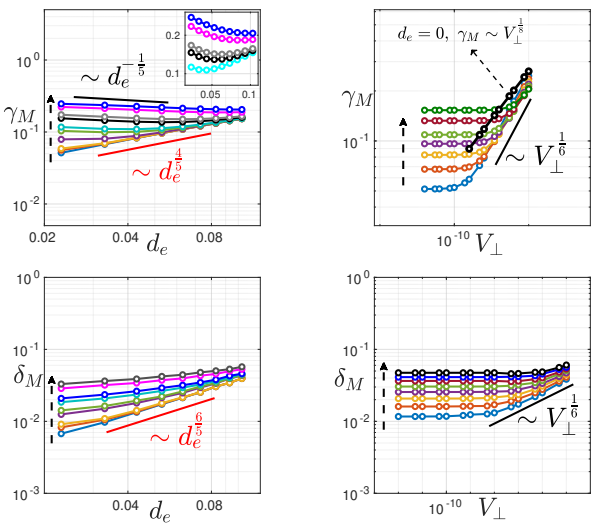

FIG. 4. Top frames: the growth rate of the fastest mode as a function of d_e (left frame) and $V_\perp$ (right frame) in $(d_e, V_\perp)$ regime. Bottom frames: the width of the reconnection layer of the fastest mode as a function of d_e (left frame) and $V_\perp$ (right frame) in $(d_e, V_\perp)$ regime. The vertical dashed arrows show the direction in which the parameter not on the x-axis increases: the parameter intervals considered are $V_\perp \in [2\times10^{-9}, 10^{-4}]$ (left frames), $d_e \in [0.023, 0.103]$ (right frames).

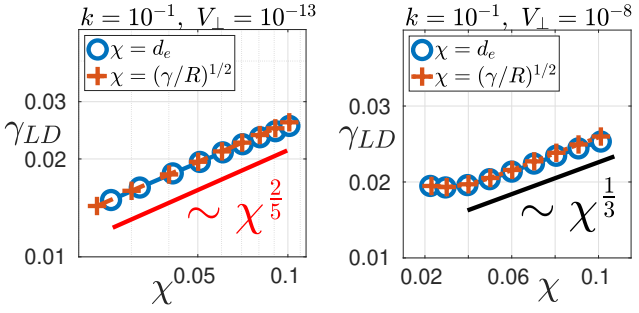

FIG. 5. Validation of the $\gamma d_e^2 \leftrightarrow R$ equivalence within the $(d_e, V_\perp)$ regime in the large-Δ' limit, knowing that it also holds across all limits. The parameter interval considered is $\chi \in [0.023, 0.103]$.

lar viscosity) can compete and make the dispersion relation appreciably depart from a power law-scaling. In some respects, this case is similar to what is met in reduced MHD, when the contributions of both electron inertia and resistivity are simultaneously retained (cf. Sec. VIII of Ref. 84) and to what is met in EMHD (cf. Sec. V B), although in these cases the parameter region in which both electron inertia and resistivity appreciably contribute is very narrow, and therefore a power-law scaling dominated by a single parameter at a time can be easily recovered. In this $(d_e, V_\perp)$ EMHD regime, instead, the region where both parameters contribute is wider, and a change of dependence on them is observed. In particular, when $V_\perp$ is kept fixed, the power-law dependence on d_e (and, similarly, on R) can even pass from a positive scaling to a negative one. This change of regime is appreciable, since, within it, the growth rate amplitude spans a variation of at least one order of magnitude: for the small-Δ' limit this is shown in the top-left frame of Fig.2.

Notice there is not any inconsistency in this result, since a further change of regime is measured as d_e further decreases, which makes the negative power-law dependence of the growth rate on d_e to "saturate" by making the negative exponent progressively tend to zero: the dependence of γ on d_e disappears when the value of the latter becomes sufficiently small, and thus the regime becomes purely viscous. This is shown in the top frames Fig.2 for the dependence of γ on d_e only. An analogous behaviour, not displayed here, is observed for R. The consistency of these numerical results is supported by the fact that the power law scalings with respect to d_e and to R, which are locally measured for the same value of $V_\perp$ in some sub-intervals of the dispersion relation, coincide via the correspondence $\gamma d_e^2 \leftrightarrow R$: for example, the negative scaling $\gamma_{SD} \sim R^{-1/3}$ with respect to R (not shown, here) obtained in a parameter interval of the $(R, V_\perp)$ tearing regime in small-Δ' limit, can be recovered by substituting $d_e \sim (R/\gamma)^{1/2}$ in the scaling $\gamma(d_e) \sim d_e^{-1/2}$ shown in the top-left frame of Fig.2. A similar procedure can be applied to the scalings of the large-Δ' limit shown in Fig. 5, where the explicit equivalence between γ_{LD} in the $(d_e, V_\perp)$ and in the $(R, V_\perp)$ regimes is highlighted via the correspondence $\gamma d_e^2 \leftrightarrow R$ at fixed values of $V_\perp$, thanks to the introduction of the variables $\chi = d_e$ and $\chi = (\gamma/R)^{1/2}$, in the inertial and resistive regimes, respectively.

Furthermore, within the parameter space considered in Fig.2-5, the scaling laws of the corresponding one-parameter regimes (i.e., purely collisionless or purely viscous) were not recovered. For instance, in the bottom-right frame of Fig.2, the green-colored line represents the scaling of γ_{LD} for the purely viscous case[9] ($\gamma_{LD} \sim V_\perp^{1/14}$), which differs from the "faster" scaling observed here, $\gamma_{LD} \sim V_\perp^{1/11}$. Similar discrepancies are visible also in the small-Δ' limit, as shown in the bottom-left frame, where the scaling[9] $\gamma_{SD} \sim V_\perp^{1/4}$ of the $d_e = 0$ case (green line) is compared with the scaling obtained in this $(d_e, V_\perp)$ case, of which the approximated estimate $\gamma_{SD} \sim V_\perp^{3/10}$ has been here shown.

Fig.4 displays the scaling laws of the growth rate γ_M and the width of the reconnecting layer δ_M for the fastest growing mode in the top and bottom frames, respectively. The left and right frames show the dependence on d_e and $V_\perp$, respectively. Upon closer examination, in the magnified part of the top-left frame of Fig. 4, we observe a dependence of γ_M on d_e, analogous to that observed in both the large and small limits of Δ' (cf. top frames of Fig.2).

The richness of behavior that we observe in EMHD, and notably the wider parameter range in which a dominance of one

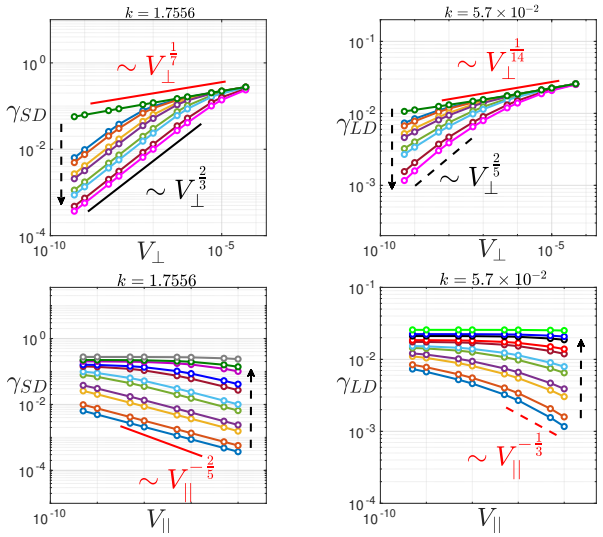

FIG. 6. Growth rates of $(V_\perp, V_{||})$ regime as function of $V_\perp$ (top frames) and as a function of $V_{||}$ (bottom frames) for small-Δ' and large-Δ' limits in the left and right frames, respectively. The vertical dashed arrows show the direction in which the parameter not on the x-axis increases: the parameter intervals considered are $V_{||} \in [5\times10^{-10}, 10^{-6}]$ (top frames) and $V_\perp \in [5\times10^{-10}, 5\times10^{-5}]$ (bottom frames).

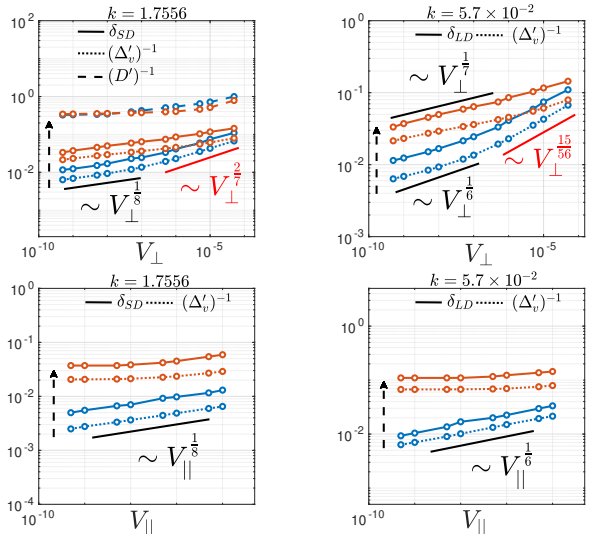

FIG. 7. Spatial scales of $(V_\perp, V_{||})$ regime as function of $V_\perp$ (top frames) and as a function of $V_{||}$ (bottom frames) for small-Δ' and large-Δ' limits in the left and right frames, respectively. The vertical dashed arrows show the direction in which the parameter not on the x-axis increases: the parameter intervals considered are $V_{||} \in [5\times10^{-10}, 10^{-6}]$ (top frames) and $V_\perp \in [5\times10^{-10}, 5\times10^{-5}]$ (bottom frames).

of the two effects is not observed, can be qualitatively related to the fact that, while in the inertial-resistive regime of both MHD (cf. Sec. VIII of Ref. 33) and EMHD (cf. Sec. V A) the "competition" between the two parameters depends on the relative amplitude of γd_e^2 vs the inverse Lundquist number S^{-1} (here corresponding to R), in the EMHD cases we consider here the transition of regime is ruled by the relative amplitude of γd_e^2 and $V_\perp/\delta^4$ in one case, and of R and $V_\perp/\delta^2$ in the other one.

C. Dependence of γ on $(V_\perp, V_{||})$

As discussed in Section III B, unlike the resistive regime where $R_\perp \propto R_{||}$ is generally true, the dimensionless parameters $V_\perp$ and $V_{||}$ can change independently, depending on the value either of the background magnetic field, or of the electron density, or of the electron temperature (cf. Eqs.(8-9]).

We now focus on a regime of experimental interest, when $V_{||}$ significantly exceeds $V_\perp$ (cf. Table II), by numerically investigating the scaling laws of the growth rate and of the width of the reconnecting layer in the large-Δ' limit, in the small-Δ' limit, and for the fastest growing mode.

These numerical results are shown in Fig.(6, 7, 8).

The ranges of $V_\perp$ and $V_{||}$ considered in the numerical calculations we have performed allow for a substantial difference in magnitude between these two non-ideal parameters, approximately of the order of 10^5. While this difference remains much smaller than those typically observed in many experiments or in space (cf. Table II), it enables us to derive scaling laws for the corresponding regimes, without necessitating wider scans with larger differences in magnitude. This choice also represents a quite good compromise from the computational point of view, since investigating regimes with extremely small values of $V_\perp$, such as those detailed in the Table II, would demand a much higher spatial resolution around the neutral line, that could be achieved for example by means of highly non-uniform grids with a larger number of points. This, in turn, could lead to ill-conditioned eigenmatrices, requiring the use of the computationally very expensive multi-precision version of the code[33].

Fig.6 illustrates the scaling of the growth rate as a function of $V_\perp$ ($V_{||}$) in the upper (lower) frames, displaying the small-Δ' and large-Δ' limits in the left and right frames, respectively. Additionally, the dependence of the growth rate on $V_\perp$ in the regime where only $V_\perp \neq 0$ is considered is shown by the dark green curves in the upper frames. Within this representation, three distinct regimes emerge: a regime where $V_\perp \gg V_{||}$ exhibiting the scaling laws of the regime[9] ($V_\perp \neq 0, V_{||} = 0$), a transition regime, and a regime where the influence of $V_{||}$ becomes manifest. These patterns hold true across the small-Δ' limit, large-Δ' limit, and for the fastest mode. The transition between the two regimes with different scalings on $V_\perp$ for the fastest growing mode limit is shown in Fig. 8. As shown in the left frames of Fig.6 and Fig.7, the scaling laws of the growth rate (γ_{SD}) and the width of the reconnecting layer (δ_{SD}) for the small-Δ' limit in the regime where the effect of $V_{||}$ is relevant have been estimated as follows:

$$\gamma_{SD} \propto V_\perp^{\frac{2}{3}} V_{||}^{-\frac{2}{5}}, \quad \delta_{SD} \propto V_\perp^{\frac{1}{8}} V_{||}^{\frac{1}{8}} \tag{17}$$

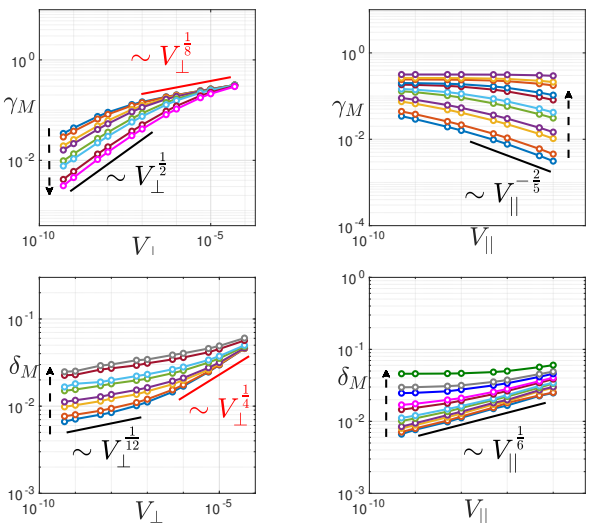

FIG. 8. Scaling laws of the growth rate γ_M (top frames) and width of reconnecting layer δ_M (bottom frames) for the fastest growing mode in $(V_\perp, V_{||})$ regime as a function of $V_\perp$ and $V_{||}$ in the left and the right frames, respectively. The vertical dashed arrows show the direction in which the parameter not on the x-axis increases: the parameter intervals considered are $V_{||} \in [5\times10^{-10}, 10^{-6}]$ (left frames) and $V_\perp \in [5\times10^{-10}, 5\times10^{-5}]$ (right frames).

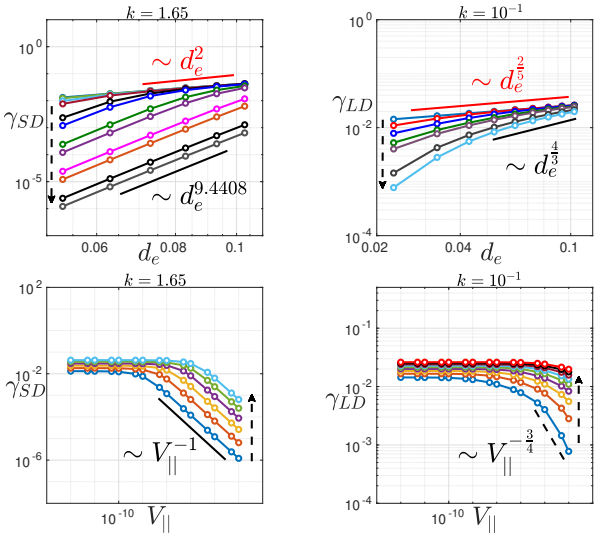

FIG. 9. Top frames: the scaling laws of the growth rate as a function of d_e for different values of $V_{||}$. Bottom frames: the scaling laws of the growth rate as a function of $V_{||}$ for different values of the electron skin depth d_e. Left frames correspond to the small-Δ' limit, while the right frames represent the large-Δ' limit in $(d_e, V_{||})$. The vertical dashed arrows show the direction in which the parameter not on the x-axis increases: the parameter intervals considered are $V_{||} \in [10^{-12}, 10^{-5}]$ (top frames) and $d_e \in [0.023, 0.103]$ (bottom frames).

while the scalings for the large-Δ' regime are estimated as

$$\gamma_{LD} \propto V_\perp^{\frac{2}{5}} V_{||}^{-\frac{1}{3}}, \quad \delta_{LD} \propto V_\perp^{\frac{1}{6}} V_{||}^{\frac{1}{6}} \tag{18}$$

In the estimates above we have omitted to note the scaling with respect to k and Δ' (cf. discussion in Sec. IV). The scalings (17-18) are represented by solid black lines in Fig. 6, Fig.7, and Fig.8, whereas those corresponding to the one-parameter regimes are drawn as solid red lines.

The negative power-law scaling of γ with respect to $V_{||}$ persists across all wavelength limits within this regime when $V_{||} \leq V_\perp$. This negative dependence seems therefore to be relevant to several scenarios of experimental interest (cf. table II).

In Fig.7, we show the scaling laws for δ (solid curves) and Δ'_v (dotted curves) across different regimes. In the upper frames we vary $V_\perp$ by considering two extreme values of $V_{||}$, namely $V_{||} = 5\times10^{-10}$ (blue curve) and $V_{||} = \times10^{-6}$ (orange curves). For the sake of clarity, curves corresponding to intermediate values of $V_{||}$ are not shown. The same approach is applied when exploring the dependence of δ on $V_{||}$ in the bottom frames of Fig.7: the $V_\perp = 5\times10^{-10}$ case and the $V_\perp = 5\times10^{-5}$ case are shown as blue and orange curves, respectively. Some comments are due, about the results shown in these figures.

First, as shown in the left frames of Fig.7, the scaling of D' is essentially independent on both $V_{||}$ and $V_\perp$ for small values, since it coincides[6] in the small-Δ' limit with the definition of Δ'; this correspondence was numerically verified in other tearing regimes[6,9]. Then we note that Δ'_v scales similarly to δ in both the small-Δ' and large-Δ' limits, as previously shown for regimes where a single non-ideal parameter at a time was considered[9]. Finally, comparing the physics in this regime to that where only $V_\perp \neq 0$ is considered, we note (cf. the top frames of Fig.6) that both γ_{SD} and γ_{LD} increase faster with $V_\perp$, when $V_{||} \neq 0$ than when $V_{||} = 0$. However, despite this faster growth in γ in both wavelength limits, the growth rate in the presence of $V_{||}$ remains smaller for a given $V_\perp$ due to its negative scaling with respect to $V_{||}$.

D. Dependence of γ on $(d_e, V_{||})$ and on $(R, V_{||})$

The emphasis in this section is on a regime where one of the parameters (i.e., d_e or R) allows for magnetic reconnection and the other one ($V_{||}$, in this case) can in principle modify it. These regimes, in which we assume $V_{||}$ to be generally much larger than $V_\perp$, are relevant to several scenarios encountered in experiments and observations (cf. Table II). We thus explore a two-parameter space, wherein the considered non-ideal parameters are either $(d_e, V_{||})$ or $(R, V_{||})$ with $R = R_\perp = R_{||}$. However, for what concerns the results shown in the following Figs[9-11], the focus will be on the collisionless case, since the scaling laws for the resistive regime can be recovered again through the correspondence $\gamma d_e^2 \leftrightarrow R$. Fig.(12), only, is devoted to the viscous-resistive regime: here the scalings of γ_{SD} are shown as a function of R and $V_{||}$ in the left and right frames, respectively.

To explore the $(d_e, V_{||})$ regime, we performed a com-

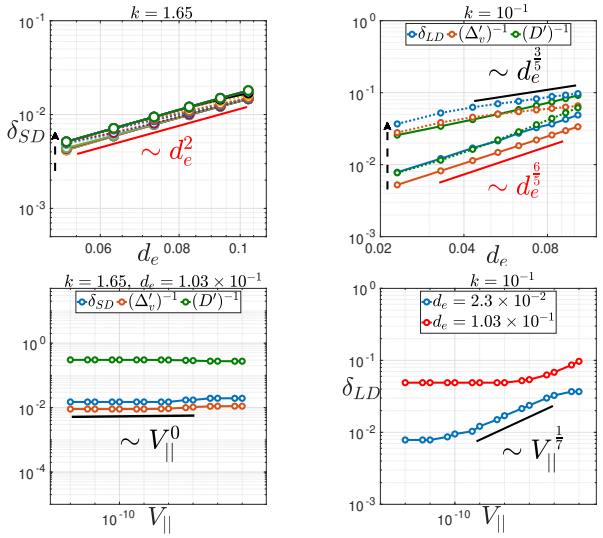

FIG. 10. Top frames: the scaling laws of the δ as a function of d_e for different values of $V_{||}$ in the left frame, and the scalings of the spatial scales for two values of $V_{||}$ in the right frame (dashed lines for $V_{||} = 10^{-6}$ and solid lines for $V_{||} = 10^{-12}$). Bottom frames: the scaling laws of the spatial scales as a function of $V_{||}$ for one value of d_e in the left frame, and the scaling of δ for two values of d_e in the right frame. Left frames correspond to the small-Δ' limit, while the right frames represent the large-Δ' limit in $(d_e, V_{||})$. The vertical dashed arrows show the direction in which the parameter not on the x-axis increases: the parameter intervals considered are $V_{||} \in [10^{-12}, 10^{-5}]$ (top frames) and $d_e \in [0.023, 0.103]$ (bottom frames).

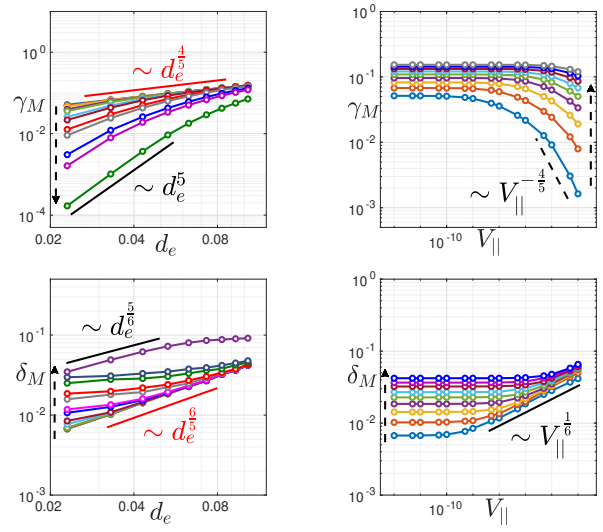

FIG. 11. Top frames: the growth rate of the fastest mode as a function of d_e (left frame) and $V_{||}$ (right frame) in $(d_e, V_{||})$ regime. Bottom frames: the width of the reconnection layer of the fastest mode as a function of d_e (left frame) and $V_{||}$ (right frame) in $(d_e, V_{||})$ regime. The vertical dashed arrows show the direction in which the parameter not on the x-axis increases: the parameter intervals considered are $V_{||} \in [10^{-12}, 10^{-5}]$ (left frames) and $d_e \in [0.023, 0.103]$ (right frames).

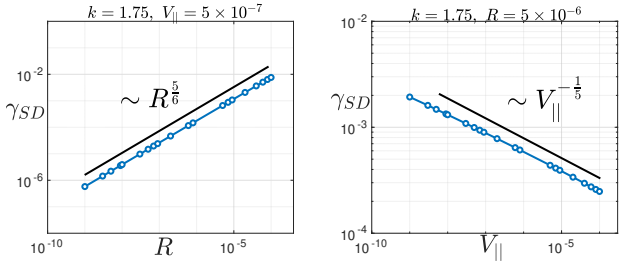

FIG. 12. Growth rates of the small-Δ' limit as function of R and $V_{||}$ for the $(R, V_{||})$ regime in the left and right frames, respectively. All other non-ideal parameters are zero.

prehensive scan across wide intervals for various non-ideal parameters and wavenumbers: $k \in [0.05, 1.85]$ with $N_k = 40$ uniformly separated values of the wavenumber, $V_{||} \in [10^{-12}, 10^{-5}]$ with $N_{V_{||}} = 15$ different values of $V_{||}$, and $d_e \in [0.023, 0.103]$ with $N_{d_e} = 9$ uniformly separated values of d_e. Fig.9 and Fig.10 illustrate the scaling laws for the growth rate and width of the inner layer, respectively. The left frames represent the small-Δ' limit, while the right frames show the large-Δ' limit. In the top frames, the dependence on d_e is shown, while the bottom frames display the quantities as a function of $V_{||}$.

Fig.9 and Fig.10 show complex behaviors. Initially, in the extreme cases where $V_{||}$ approaches very small values, the growth rates display a dependence on d_e of the kind $\gamma_{SD} \propto d_e^2$ and $\gamma_{LD} \propto d_e^{2/5}$. These scalings, shown in the top frames of Figs.9, coincide with those found in the purely collisionless regime[9]. However, deviations from this regime appear at the increase of $V_{||}$ in both wavelength limits, although this deviation is more evident in the small-Δ' limit for what concerns the dependencies on both d_e and $V_{||}$. The large-Δ' limit exhibits more intricate behavior where no clear power law as a function of $V_{||}$ is observed. Although scanning intervals with larger values of $V_{||}$ and d_e could potentially describe a regime characterized by well-defined power laws in the large-Δ' limit, we chose not to explore this due to its lack of practical interest, at least according to the estimates provided in Table II. Based on the numerical results we obtained, the best approximation for the scaling laws in the small-Δ' and large-Δ' limits seem to be, respectively,

$$\gamma_{SD} \propto d_e^{9.4} V_{||}^{-1}, \quad \delta_{SD} \propto d_e^2, \tag{19}$$

$$\gamma_{LD} \propto d_e^{\frac{4}{3}} V_{||}^{-\frac{3}{4}}, \quad \delta_{LD} \propto d_e^{\frac{3}{5}} V_{||}^{\frac{3}{5}}. \tag{20}$$

Again, we omitted in the equation above the scalings with respect to k and Δ', which at this level of preliminary analysis would require a much larger computational effort, in order to grant the convergence of the solution in the whole parameter range considered. Some additional comments can be then made, about Eqs. (19-20). First, similarly to the anisotropic-viscous regime discussed in Section V C, the growth rate exhibits a negative power-law relationship with respect to $V_{||}$ in

all limits —indicating a decrease in the growth rate as $V_{||}$ increases. Moreover, similar to the small-Δ' limit of the warm reduced-MHD regime[6], the width of the inner layer in the small-Δ' displays no dependence on $V_{||}$. In the large-Δ' limit, instead, a non-trivial dependence on $V_{||}$ is recovered.

Finally, Fig.11 displays the scaling laws of γ_M and δ_M (fastest growing mode) in the top and bottom frames, respectively. Once more, we observe that the dependence on $V_{||}$ is not monotonic, since it is negligible for small values of the parameter, while it becomes more important as $V_{||}$ increases. The scaling laws for the fastest mode have been approximately estimated to be

$$\gamma_M \sim d_e^5 V_{||}^{-\frac{4}{5}}, \quad \delta_M \sim d_e^{\frac{5}{6}} V_{||}^{\frac{1}{6}}. \tag{21}$$

The left frames of Fig.11 indicate that the scaling laws of the purely collisionless regime (i.e., $\gamma_M \sim d_e^{4/5}$ and $\delta_M \sim d_e^{6/5}$) are recovered for small enough values of $V_{||}$. In principle, the negligibility of $V_{||}$ is expected when $\gamma d_e^2 |\psi''| \gg V_{||} |b^{(iv)}|$.

This may be translated into a condition on the characteristic scales at play. To this end, we could use the heuristic estimates outlined in Ref. 9, which in a generic wavelength limit can be written as $\psi'' \sim \psi D'/\delta$ and $b^{(iv)} \sim b/\delta^4$, combined with the further heuristic estimate $b/\psi \sim \gamma/(k\delta)$ (which has been verified in several reconnection regimes[6,9,33]). This would lead us to read the condition $\gamma d_e^2 |\psi''| \gg V_{||} |b^{(iv)}|$ as $k d_e^2 D' \delta^4 \gg V_{||}$, whose verification would however require a more accurate knowledge of the scalings (19-21) with respect to the (inverse) wavelength k. The numerical investigations performed in this work, suggest however this to be not an easy task: in presence of a non negligible parallel viscosity $V_{||}$, the value of k appears to determine here the regime of reconnection in the different wavelength limits, in a way which is more constraining than what is normally met in other reconnection regimes (cf., in this regard, also Sec. VI B and the concluding remarks in Sec. VII). That is, a certain functional dependence (e.g., a power law-like scaling) for a given interval of the non-ideal parameters seems, in presence of viscosity, to be valid in a narrower wavelength interval than what happens in other reconnection regimes met in EMHD. This can be understood because of the higher order of the derivative weighting the effect of $V_{||}$ than that weighting the other non-ideal terms: for example, while the comparison of the inertial and resistive effects leads one to compare $\gamma(k) {d_e}^2$ and R, the comparison of, e.g., the inertial and viscous effects leads one to the comparison above between $k {d_e}^2 D'(k) \delta^4(k)$ and $V_{||}$. At the same time, the restriction to a specific wavelength limit is bound to the further comparison of the product $\Delta'(k)\delta(k)$ with 1. As a result, while the dominance, e.g., of a fully resistive or of a fully inertial regime may span a quite wide wavelength regime to the point that the an inertia-dominated or a resistivity-dominated regime can be observed, for fixed non-ideal parameters, both in the small- and large-Δ' limits, the transition between regimes where $V_{||}$ dominates or is negligible with respect to fixed d_e or R may occur in a narrower wavelength interval. Also note that this effect is more pronounced for $V_{||}$ than in presence of $V_\perp$ (cf. Sec. V B), because the relative importance of the perpendicular viscosity displays a weaker dependence on the spatial scales than $V_{||}$: the comparison between inertial effects and those related to $V_\perp$ leads indeed us to compare $\gamma {d_e}^2 |\psi_1''|$ with $V_\perp |\psi_1^{(iv)}|$ and, therefore, using arguments similar to those above, to compare $\gamma(k) {d_e}^2 D'(k) \delta^3(k)$ with $V_\perp$.

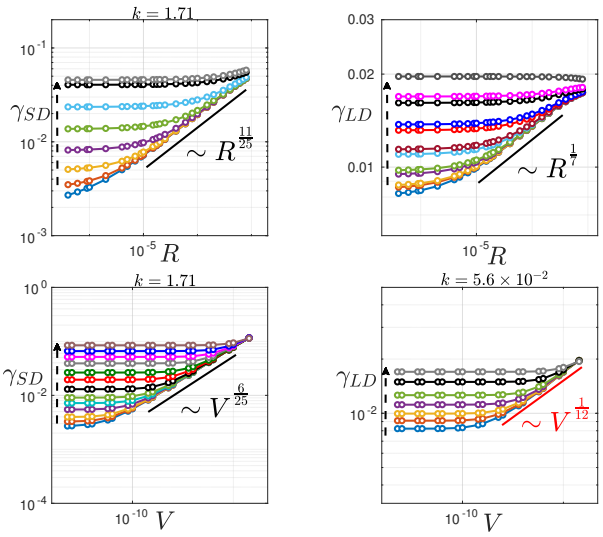

FIG. 13. Top frames: the scaling laws of the growth rate as a function of R for different values of V. Bottom frames: the scaling laws of the growth rate as a function of V for different values of R. Left frames correspond to the small-Δ' limit, while the right frames represent the large-Δ' limit in $(d_e = 0.023, R, V)$ regime. The vertical dashed arrows show the direction in which the parameter not on the x-axis increases: the parameter intervals considered are $V \in [6\times10^{-14}, 6\times10^{-5}]$ (top frames) and $R \in [4\times10^{-7}, 10^{-3}]$ (bottom frames).

The scaling laws expressed by Eqs.(21) apply indeed in a finite interval of values of $V_{||}$. Additionally, the bottom-left frame of Fig.11 exhibits a complete change of convexity of the $\gamma(d_e)$ dependence, indicating the presence of a critical value $V_{||,c}$ for which the width of the reconnection layer displays a very weak dependence on d_e (and for which, the estimates of Eqs. (21) cease to be valid).

VI. TEARING MODES WITH A MORE THAN TWO-PARAMETERS DEPENDENCE

Let us now turn the attention to more realistic cases, in which all non-ideal parameters considered in the model of Eqs. (1-2) are retained, by considering values whose relative orderings are compatible with the cases displayed in Table II.

A. Dependence of γ on $d_e = const$, $R_\perp = R_{||} = R$ and $V_\perp = V_{||} = V$

We first consider for simplicity the case where d_e remains constant while exploring the scaling laws for isotropic resistivity and viscosity. The reason why the $d_e = const$ case can

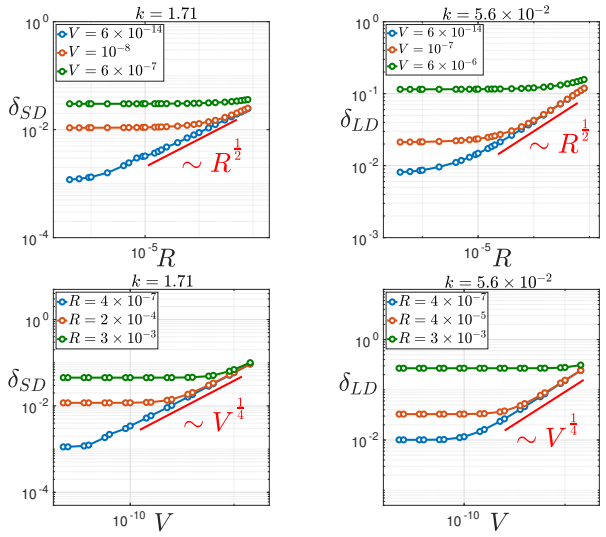

FIG. 14. Top frames: the scaling laws of the δ as a function of R. Bottom frames: the scaling laws of δ as a function of V. Left frames correspond to the small-Δ' limit, while the right frames represent the large-Δ' limit in $(d_e = 0.023, R, V)$ regime.

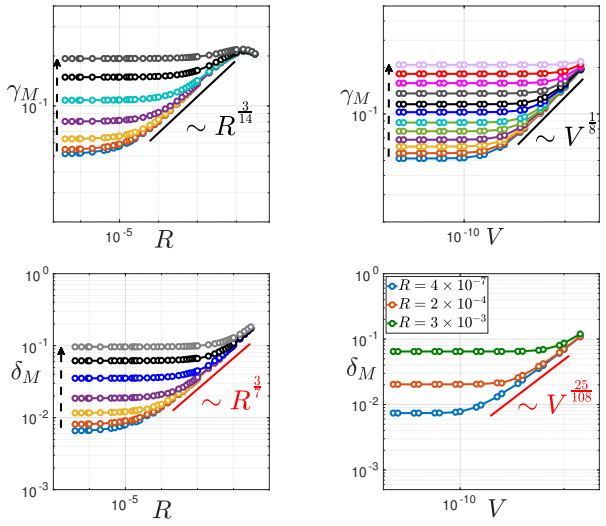

FIG. 15. Top frames: the growth rate of the fastest mode as a function of R (left frame) and V (right frame) in $(d_e = 0.023, R, V)$ regime. Bottom frames: the width of the reconnection layer of the fastest mode as a function of R (left frame) and V (right frame) in $(d_e = 0.023, R, V)$ regime. The vertical dashed arrows show the direction in which the parameter not on the x-axis increases: the parameter intervals considered are $V \in [6\times10^{-14}, 6\times10^{-5}]$ (left frames) and $R \in [4\times10^{-7}, 3\times10^{-3}]$ (right frames).

be physically interesting is due to the fact that the applicability of the model is limited by the small scale separation between the ion and the electron skin depth (i.e. $d_e/d_i = \sqrt{m_e/m_i}$ for Hydrogen) and by the constraint on the spatial scales $\ell \leq d_i$. However, varying d_e can also relate to changes in the plasma species, thereby implying the dependence of the growth rate on the considered plasma and on its degree of ionization. In

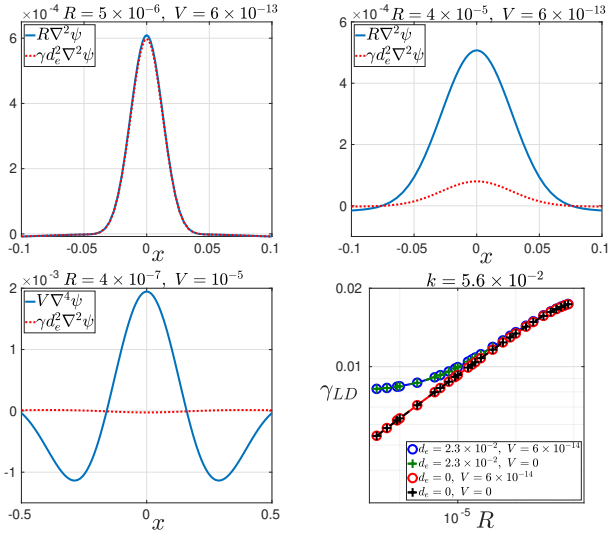

FIG. 16. Top frames and bottom-left frame: the contributions of the collisionless and resistive terms for different values of R and V. Bottom-right frame: the scaling law of γ in the large-Δ' limit for four cases, chosen so to emphasize the effects of changing d_e and V on the system: (similar behavior also holds in the small-Δ' limit and the fastest mode regime).

general, heavier ions imply that larger values of d_e must be considered (possibly departing from the asymptotic tearing regime, as d_e becomes larger than[85] ~ 0.1), unless each of the heavier ions is not completely ionized: this allows for a large scale separation between d_e and d_i, implying that values up to $\sim 1/\sqrt{Z}$ smaller of d_e can considered, provided that $a = \bar{d}_i$ is assumed (cf. discussion below Eq. (11), in Sec. III B).

In the regime we consider here, the value $d_e = 0.023$ represent a hydrogen plasma, under the hypothesis that $L_0 = a = d_i$. Fig.13 (and Fig.14) shows the numerical scaling of γ (and of δ) as a function of both $R_\perp = R_{||} = R$ and $V_\perp = V_{||} = V$ in the top and bottom frames, respectively. The left frames illustrate the scaling in the small-Δ' limit, while the right frames show the scalings in the large-Δ' limit. In the parameter interval considered, the scalings in the small-Δ' limit have been estimated to be

$$\gamma_{SD} \propto R^{\frac{11}{25}} V^{\frac{6}{25}}, \quad \delta_{SD} \propto R^{\frac{1}{2}} V^{\frac{1}{4}}, \tag{22}$$

while the scalings in the large-Δ' limit are approximated as

$$\gamma_{LD} \propto R^{\frac{1}{7}} V^{\frac{1}{12}}, \quad \delta_{LD} \propto R^{\frac{1}{2}} V^{\frac{1}{4}}. \tag{23}$$

A close look at Fig.13 reveals a deviation from the expected scaling laws for the purely resistive case. However, the numerical scaling obtained for the dependence on V is almost equal to that satisfied in the purely viscous regime, where $\gamma_{SD} \sim V^{1/4}$ and $\gamma_{LD} \sim V^{1/12}$. To understand this discrepancy, in Fig.16 we plot the profiles of the terms allowing for the breaking and reconnecting of the field lines, namely $\gamma d_e^2 \nabla\psi$, $R\nabla^2\psi$, and $V\nabla^4\psi$, respectively. The cases therein displayed correspond to the values of $k = 0.05$ and of $(R = 5\times10^{-6}, V = 6\times10^{-13})$, of $(R = 4\times10^{-4}, V = 6\times10^{-13})$,

and of $(R = 4\times10^{-7}, V = 10^{-5})$. These are shown in the top-left, top-right, and bottom-left frames of Fig.13, respectively.

The contribution of the collisionless term (i.e., the one depending on d_e^2) is evident in the top frames, while it becomes negligible in the bottom-left frame. This explains the deviation of the scalings from the power laws in the purely resistive regime. Concerning the width of the reconnection layer, shown in Fig.14, we recover the scalings for both purely resistive and purely viscous regimes for the extreme values of the V parameter: the dependence on R alone is recovered for very small values of V, and the dependence on V alone is recovered for very small values of R.

For larger values of the non-ideal parameters, the deviations from power-law scalings become more pronounced. Additionally, we observe that the qualitative behavior of the power-law scalings obtained here with respect to R and V are not significantly affected by changing the numerical value of d_e or by extending the intervals of R and V considered here. In summary, in the bottom-right frame of Fig.16, the variation of γ_{LD} as a function of R for four cases illustrates the role played by d_e in amplifying the growth rate. This feature is common to all wavelength limits (i.e., also in the small-Δ' limit and for the fastest growing mode).

Finally, in Fig.15, we plot the scalings of the fastest mode as function of R and V in the left and right frames, respectively. In the range where a power law can be identified, this has been approximately estimated to be close to

$$\gamma_M \propto R^{\frac{3}{14}} V^{\frac{1}{8}}, \quad \delta_M \propto R^{\frac{3}{7}} V^{\frac{25}{108}} \tag{24}$$

Within the incertitude of these estimates, we can nevertheless quantify an appreciable discrepancy with respect to the power-law scaling of γ_M expected in the purely resistive regime ($\gamma_M \sim R^{2/7}$) or in the viscous regime ($\gamma_M \sim V^{17/108}$). Curiously, however, the width of the reconnecting layer δ_M of Eq. (24) displays a power law-scaling, which is apparently compatible with the product of those found in the purely resistive ($\delta_M \sim R^{3/7}$) and purely viscous ($\delta_M \sim V^{25/108}$) isotropic regimes[9].

B. Dependence of γ on $R_{||} \sim R_\perp/2$ and $R_\perp \sim V_{||} \gg V_\perp$ for $d_e \sim$ *constant*

We finally consider, as an example of possible relevance to natural plasmas or laboratory plasmas in magnetically confined helicon-type devices, the case $R_{||} \sim R_\perp/2$ and $R_\perp \sim V_{||} \gg V_\perp$ for $d_e \sim$ *constant*. In this scenario, we consider $d_e = 0.0531$, a value that is relevant for some cases reported in table II, when $L_0 = a = d_i$ is assumed. The intervals of variation for $R_\perp = 2R_{||}$ and $V_{||}$ are $[4\times10^{-9}, 10^{-5}]$ and $[10^{-12}, 10^{-6}]$, respectively. These parameter ranges encompass various cases detailed in Table II.

Figs.17-19 show the results of the numerical integration in this regime. The scalings of γ and δ in all wavelength limits reveal a weaker dependency on $R_\perp$ than in the in the $(R, V_{||})$ case. This can be attributed to the effect of a non-null electron inertia. Only a narrow transition region is observed when the

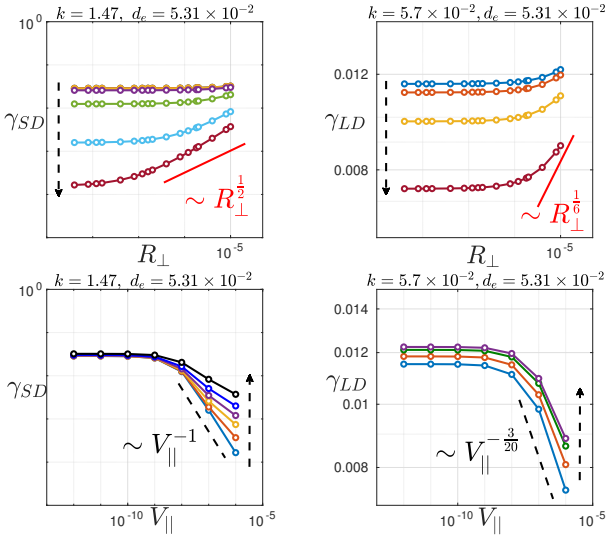

FIG. 17. Top frames: the scaling laws of the growth rate as a function of $R_\perp$ for different values of $V_{||}$. Bottom frames: the scaling laws of the growth rate as a function of $V_{||}$ for different values of $R_\perp$. Left frames correspond to the small-Δ' limit, while the right frames represent the large-Δ' limit in $(d_e = 0.0531, R_\perp = 2R_{||}, V_{||}, V_\perp = 0)$ regime. The vertical dashed arrows show the direction in which the parameter not on the x-axis increases: the parameter intervals considered are $V_{||} \in [10^{-12}, 10^{-6}]$ (top frames) and $R_\perp \in [4\times10^{-9}, 10^{-5}]$ (bottom frames).

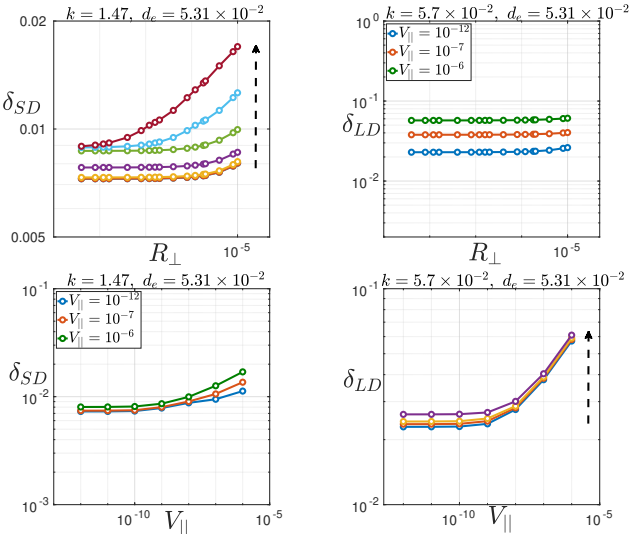

FIG. 18. Top frames: the scaling laws of the width of the inner layer as a function of $R_\perp$ for different values of $V_{||}$. Bottom frames: the scaling laws of the width of the inner layer as a function of $V_{||}$ for different values of $R_\perp$. Left frames correspond to the small-Δ' limit, while the right frames represent the large-Δ' limit in $(d_e = 0.0531, R_\perp = 2R_{||}, V_{||}, V_\perp = 0)$ regime. The vertical dashed arrows show the direction in which the parameter not on the x-axis increases: the parameter intervals considered are $V_{||} \in [10^{-12}, 10^{-6}]$ (top frames) and $R_\perp \in [4\times10^{-9}, 10^{-5}]$ (bottom frames).

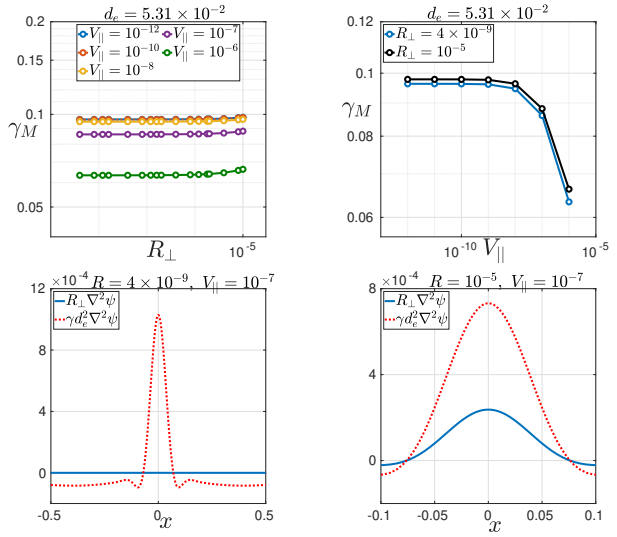

FIG. 19. Top frames: the scaling laws of the growth rate of the fastest mode as a function of $R_\perp$ (left frame) for different values of $V_{||}$ and as a function of $V_{||}$ in the right frame in $(d_e = 0.0531, R_\perp = 2R_{||}, V_{||}, V_\perp = 0)$ regime.. Bottom frames: the contributions of the collisionless and resisitive terms for different values of R and V.

resistive term becomes non-negligible, as it is illustrated in the top frames of Fig.17 and in the top-left frame of Fig.19.

The power law scaling laws estimated here in both small-Δ' and large-Δ' limits indicate that the purely collisionless reconnection regime represents an accurate approximation for the smaller values of $V_{||}$ and $R_\perp$, studied in this section. However, for larger values of $V_{||}$, the dynamics is predominantly governed by $R_\perp$ and by $V_{||}$ (cf. Section V D).

As $R_\perp$ reaches larger values, let us say around 5×10^{-6}, the influence of resistive effects becomes evident. Interestingly, this feature is not observed in the scalings of the fastest mode, which are shown in the top frames of Fig.19: here the dependence of the fastest mode on $R_\perp$ appears to be almost negligible. This suggests that the the fastest mode be dominated by inertial effects and by the parallel viscosity alone.

The strong influence of the term of the linearized equations, which is related to electron inertia, is highlighted in the bottom frames of Fig.19. Here we plot both $\gamma d_e^2 \nabla^2 \psi$ (represented by dotted red curves) and the resistive contribution $R_\perp \nabla^2 \psi$ (solid blue curve) for two cases, respectively corresponding to the smallest and largest values of $R_\perp$. In both cases, the contribution from the collisionless term is much larger than that of the resistive term. It must be however taken into account that for large values of $R_\perp$ (bottom-right frame of Fig. 19), the resistive contribution can alter the scaling laws, and can thus lead to a deviation from the scalings obtained in the purely collisionless regime. Although in the bottom frames of Fig.19 is shown just the large-Δ' limit, the behavior remains qualitatively the same in the small-Δ' limit and in the fastest mode regime.

VII. CONCLUSIONS

In this study, we investigated the linear dynamics of tearing modes in slab non-relativistic EMHD across ranges of non-ideal parameters relevant to both laboratory plasmas and possibly of interest to astrophysical ones. This analysis extends that of several previous works (see Ref.[9] and references therein), in which the dependence of the dynamics on a single non-ideal parameter was considered. Here, two or more non-ideal parameters at a time have been retained, instead.

As a general remark of "operational" kind, we first note that the characteristic scale lengths $(\Delta'_v)^{-1}$ and δ have been verified to exhibit the same scaling in the parameter spaces explored in all reconnection regimes and in all wavelength limits. This has important implications from the numerical/theoretical point of view, especially in the small-Δ' limit, where accurately determining the width of the reconnection region can be numerically challenging. The proportionality $\delta \propto \Delta'_v$ allows us in principle to determine more easily the asymptotic scaling of δ, since the numerical experience maturated with the present solver indicates that the convergence is granted more easily for the evaluation of Δ'_v than for the evaluation of δ, defined as the distance from the neutral line of the inflection point of the perturbed current density[6]. Moreover, once the proportionality factor $p = \delta/\Delta'_v$ is estimated through linear analysis for a specific reconnection regime, it may be relatively easier to to use the definition of Δ'_v, so to evaluate the reconnection layer width in nonlinear simulations, at the end of the linear phase of tearing instabilities.

Turning now the attention to the more specific results, in the inertial-resistive regime (d_e, R) discussed in Section V A, the scalings of the purely resistive and purely collisionless regimes have been recovered for $R \gg \gamma d_e^2$ and $R \ll \gamma d_e^2$, respectively, similarly to what was observed[33] in reduced MHD. However, differently from the reduced-MHD case, the transition region between these two limit regimes, where power-law scalings cease to be valid, is not narrow in the parameter space and might include experimental cases of interest, as it can be deduced from Tables I-II.

In the inertial-viscous regime $(d_e, V_\perp)$ investigated in Section V B, the scaling laws obtained in the one-parameter cases $(d_e = 0, V_\perp \neq 0)$ and $(d_e \neq 0, V_\perp = 0)$ were not recovered in the extreme limits of the considered parameter space. Notably, a non-trivial dependence on the non-ideal parameters at play −to the best of our knowledge, of a kind not yet identified in any other linear tearing regime so far analytically or numerically studied− has been found in a wide region of the parameter space: in all the small-Δ', large-Δ', and fastest mode wavelength limits, a negative power-law dependence of the growth rate on d_e has been observed in the parameter interval. Nevertheless, such a behaviour remains consistent with the requirement $\gamma \to 0$ ad $d_e \to 0$, since the dependence of γ on d_e tends to increase again until it becomes $\gamma \sim d_e^0$ and a purely viscous regime is recovered. At the same time, as shown in Table II, the effect of d_e should not be neglected in many cases of experimental evidence, where it is often many orders of magnitude larger than $V_\perp$. In general, the importance of $V_\perp$ should not be underestimated, in particular, in some scenarios when

the width of the reconnecting layer becomes extremely small ($\delta \ll 1$): this can lead to a large contribution from the term associated with perpendicular hyper-viscosity in the model, i.e., $V_\perp(\partial^4\psi/\partial x^4)|_{x\sim\delta} \sim V_\perp(\psi|_{x\sim\delta})/\delta^4$.

As discussed in Section III B, in plasma scenarios where Braginskii model holds, $V_\perp$ and $V_{||}$ can independently vary. This differs from the case of $R_\perp$ and $R_{||}$, which differ just by a numerical factor that depends on the plasma under consideration. Therefore, investigating the purely anisotropic viscous regime ($V_\perp, V_{||}$) becomes theoretically interesting. This was performed in Section V C. In Ref.9, it was demonstrated that the growth rate generally increases, in the asymptotic limit, at the increase of an isotropic viscosity $V = V_\perp = V_{||}$. However, in the two-parameter purely (anisotropic) viscous case studied in Section V C, this pattern no longer holds true and the scalings of both γ and δ on $V_\perp$ in all wavelength limits are generally different from that obtained[9] when the ratio $V_\perp/V_{||}$ is kept constant. The growth rate exhibits a negative scaling in $V_{||}$ in all wavelength limits when $V_{||} \geq V_\perp$. This happens both when $V_{||} \gg V_\perp$ and when $V_{||}$ is smaller than $V_\perp$ but not negligible with respect to it. In the same parameter interval, no negative dependency on $V_{||}$ was observed for δ.

In several practical scenarios highlighted in Table II, R, d_e, and $V_{||}$, are likely to be simultaneously accounted for. Only in some parameter interval it's plausible to neglect one or even two of these parameters, thereby falling back to the one-parameter regimes. In many other situations, instead, these three parameters (or a combination of two of them) must not be neglected. As discussed in Section V D, in the ($d_e, V_{||}$) regime or, similarly ($R, V_{||}$), for sufficiently small values of the parallel hyperviscosity we recovered the scalings respectively observed in the purely collisionless and purely resistive regime. However, for larger values of $V_{||}$, similar to happens in the ($V_\perp, V_{||}$) regime, we observed a negative dependency of the growth rate on $V_{||}$ across all considered wavelength limits. Notably, in the small-Δ' limit of this regime, the width of the reconnecting layer δ_{SD} seems to be independent of $V_{||}$. This behaviour appears to be similar to that of the reconnecting layer width in the small-Δ' limits of the warm-collisionless or of the warm-resistive reduced MHD regimes, where δ_{LD} is found[6,33] not to depend on the ion-sound Larmor radius ρ_s (similarly to the $V_{||}$, here), but just on the electron inertia or on the resistivity, respectively which therein allow the onset of reconnection, so as $V_\perp$ does here.

We then considered in Sec. VI A an example of a three-parameter dependence corresponding to a Hydrogen plasma for which we assumed an arbitrary normalized value $d_e = 0.023$ for the electron skin depth (corresponding to $L_0 = a = d_i$), and in which we kept account of an isotropic resistivity ($R = R_{||} = R_\perp$) and of a isotropic hyper-viscosity $V = V_\perp = V_{||}$. We thus identified a new tearing regime characterized by scaling laws, which appreciably deviate from those observed in the one-parameter or two-parameter regimes that could be in principle associated to this case of study, if only one or two parameters at a time were retained. More in general, depending on the relative amplitudes of the different terms capable of breaking the topology of the magnetic fields, different tearing mode regimes, not always displaying clear power-law scalings, can be observed −cf. Fig.16.

Finally, a more realistic regime of potential experimental and observational significance (i.e., $V_{||} \gg V_\perp \neq 0$, $R_\perp = 2R_{||}$, and $d_e = 0.0513$ −cf. Table I-II), was investigated in Section VI B. Here we observed again the negative scaling of the growth rate with respect to $V_{||}$ in a significant interval of the parameter space: a behavior that seems to be universal in this EMHD model, as long as an anisotropic (i.e., two-parameter) hyper-viscosity is considered. In the scenario considered in Sec. VI B, the contribution of the collisionless (i.e., inertial) effects dominates, while that of $R_\perp$ (and thus of $R_{||}$) becomes significant only for quite large values of $R_\perp$ (i.e., for $R_\perp > 10^{-5}$ in the considered case of $d_e \simeq 0.05$). An important result, suggested also by the cases of study of previous sections, was here more evidently confirmed: distinct wavelength limits can be governed by entirely different reconnection regimes. This is evident, for example if one compares the growth rates of the small-Δ' limit (the red curve at the bottom of the top-left frame in Fig.17) with the growth rate of the fastest mode (the green curve in the top-left frame of Fig.19), for the values $R_\perp = 10^{-5}$, $d_e = 0.0531$, and $V_{||} = 10^{-6}$: in the small-Δ' limit a significant contribution comes from the resistive term and considerably affects the scalings. Conversely, the fastest mode appears to be entirely collisionless, with a wholly negligible contribution from resistivity throughout all parameter intervals investigated.

Two important conclusions, follow from all this.

First, in general, determining whether to neglect or not a non-ideal parameter in tearing mode analysis is not always straightforward nor simple. This especially true for cases of practical interest, since the result may strongly depend on the wavelength of interest, especially when the relevant non-ideal parameters are weighted by higher order derivatives: the weight of each non-ideal term in the tearing mode dynamics depends on the order of the derivatives of the eigenfunction it is applied to. This is trivially why, in general, different reconnection "regimes", meant as different dependencies of γ on the non-ideal parameters, even when they are made vary in the same intervals, exist for different wavelength ranges. Viscosity effects, however, entering with a fourth order derivative either of ψ_1 (i.e., for viscosity effects related to $V_\perp$) or of b_1 (i.e., for viscosity effects related to $V_{||}$), make intervene higher powers of the characteristic gradient scales δ, in the comparison of the weight of the different non-ideal terms. This implies a stronger dependence on k, due to the general dependence $\delta(k)$, which is specific of the small/large-Δ' and fastest mode regime. At the same time, the effects of $V_{||}$ in this sense seem to be stronger than those of $V_\perp$, due to the further dependence on k introduced by the ordering $|b_1/\psi_1| \sim \gamma(k)/(k\delta(k))$ (cf. Sec. V D and VI). Because of this, when accounting for electron viscosity EMHD tearing mode may display "clear" power-law scalings only in quite narrower wavelength intervals, compared to other examples of tearing modes, e.g. in reduced MHD. As a side consequence, this means that numerical dissipation effects, whose a-priori "control" in the simulation may be not easy (e.g., when it is difficult to quantify them in terms of an equivalent viscosity or resistivity), may have non-evident implications for the linear evolution of tearing

type instabilities, especially in low collision regimes: the interpretation of the numerical results may then require to keep account of these effects.

Then, it seems that electron inertia and parallel electron viscosity dominate the linear dynamics of tearing-type instabilities on some large aspect ratio current sheets, even when the resistivity may be not negligible for small-Δ' tearing modes developing on the same structures. Since large aspect ratio current sheets are relevant to turbulence reconnection, this suggests that collisionless dissipation may be a dominant feature of reconnection in turbulent plasmas at the electron-only (EMHD) scales. However, stronger statements in this regard require first one to investigate how this scenario may change in presence of sheared flows parallel to the neutral line (cf. discussion in Sec. II A of Ref. 9). This will be the subject of some future work.

ACKNOWLEDGMENTS

The authors are grateful to Daniel Medina Roque and Yu Chun Li for the their M1 internship report[86], in which they collected and compared the plasma parameters of several helycon devices: the bibliographic research they conducted was much helpful to us for the construction of Tables I-II. Useful discussions with Guilhem Dif-Pradalier (IRFM-CEA) are also gratefully acknowledged.

This work has received financial support from the AIM4EP project (ANR-21-CE30-0018), funded by the French National Research Agency (ANR). A part of this work has been also carried out within the framework of the French Federation for Magnetic Fusion Studies (FR-FCM) and of the Eurofusion consortium, and has received funding from the Euratom research and training programme 2014-2018 and 2019-2020 under grant agreement No 633053 (WPEDU fundings obtained through FR-FCM AAP 2017-2021 "Evolution of current sheets in low-collision plasmas", in particular, are gratefully acknowledged). The views and opinions expressed herein do not necessarily reflect those of the European Commission.

VIII. DATA AVAILABILITY

The data that supports the findings of this study are available within the article.

[1] S. Kingsep, K. V. Chukbar, and V. V. Yan'kov, "Electron magnetohydrodynamics," **16** (1990).
[2] A. V. Gordeev and L. I. Kingsep, A. S.and Rudakov, "Electron magnetohydrodynamics," Physics Reports **243**, 215–315 (1994).
[3] N. Attico, F. Califano, and F. Pegoraro, "Fast collisionless reconnection in the whistler frequency range," Phys. Plasmas **7**, 2381–2387 (2000).
[4] D. Biskamp, *Magnetic reconnection in plasmas* (Cambridge University press, Cambridge, UK, 2000).
[5] H. P. Furth, J. Killeen, and M. N. Rosenbluth, "Finite-resistivity instabilities of a sheet pinch," Phys. Fluids **6**, 459–484 (1963).
[6] H. Betar, D. Del Sarto, M. Ottaviani, and A. Ghizzo, "Microscopic scales of linear tearing modes: a tutorial on boundary layer theory for magnetic reconnection," Journal of Plasma Physics **88**, 925880601 (2022).
[7] Y. Kuramitzu, T. Moritaka, Y. Sakawa, T. Morita, T. Sano, M. Koenig, C. D. Gregory, N. Woolsey, K. Tomita, H. Takabe, Y. L. Liu, S. H. Chen, and M. Matsukiyo, S. amd Hoshino, "Magnetic reconnection driven by electron dynamics," Nature Comm. **9**, 5109 (2018).
[8] T. D. Phan, J. P. Eastwood, M. A. Shay, J. F. Drake, B. U. Sonnerup, M. Fujimoto, P. A. Cassak, M. Øieroset, J. L. Burch, R. B. Torbert, A. C. Rager, J. C. Dorelli, D. J. Gershman, C. Pollock, P. S. Pyakurel, C. C. Haggerty, Y. Khotyaintsev, B. Lavraud, Y. Saito, M. Oka, R. E. Ergun, A. Retino, O. Le Contel, M. R. Argall, B. L. Giles, T. E. Moore, F. D. Wilder, R. J. Strangeway, C. T. Russell, P. A. Lindqvist, and W. Magnes, "Electron magnetic reconnection without ion coupling in Earth's turbulent magnetosheath," Nature **557**, 202–206 (2018).
[9] H. Betar and D. Del Sarto, "Asymptotic scalings of fluid, incompressible "electron-only" reconnection instabilities: Electron-magnetohydrodynamics tearing modes," Physics of Plasmas **30**, 072111 (2023).
[10] A. V. Gordeev and L. I. Rudakov, "Instability of a plasma in a strongly inhomogeneous magnetic field," Zh. Exsp. Teor. Fiz. **55**, 2310 (1968).
[11] A. V. Gordeev, "Stability of a plasma contained by a strongly non-uniform magnetic field," Nucl. Fusion **10**, 319 (1970).
[12] E. V. Appleton and J. A. Ratcliffe, "Some simultaneous observations on downcoming wireless waves," Proceedings of the Royal Society of London. Series A, Containing Papers of a Mathematical and Physical Character **128**, 133–158 (1930).
[13] A. D. M. Walker, "The theory of whistler propagation," Reviews of Geophysics **14**, 629–638 (1976).
[14] R. A. Helliwell, *Whistlers and related ionospheric phenomena* (Courier Corporation, 2014).
[15] R. L. Stenzel, "Whistler waves in space and laboratory plasmas," J. Geophys. Res.: Space Phys. **104**, 14379 (1999).
[16] R. L. Stenzel, "Whistler modes excited by magnetic antennas: A review," Physics of Plasmas **26**, 080501 (2019).
[17] J. P. Klozenberg, B. McNamara, and P. C. Thonemann, "The dispersion and attenuation of helicon waves in a uniform cylindrical plasma," J. Fluid. Mech. **21**, 545 (1965).
[18] L. C. Garcia de Andrade, "Riemannian geometry of twisted magnetic flux tubes in almost helical plasma flows," Phys. Plasmas **13** (2006).
[19] M. R. Stoneking, M. A. Growdon, M. L. Milne, and R. T. Peterson, "Poloidal $e \times b$ drift used as an effective rotational transform to achieve long confinement times in a toroidal electron plasma," Phys. Rev. Lett. **92**, 095003 (2004).
[20] J. P. Kremer, T. S. Pedersen, R. G. Lefrancois, and Q. Marksteiner, "Experimental confirmation of stable, small-debye-length, pure-electron-plasma equilibria in a stellarator," Phys. Rev. Lett. **97**, 095003 (2006).
[21] P. Costello and P. Helander, "Stability of electron plasmas in stellarators," J. Plasma Phys. **89**, 935890402 (2023).
[22] N. Jain and A. S. Sharma, "Electron-scale nested quadrupole Hall field in Cluster observations of magnetic reconnection," in *Annales Geophysicae*, Vol. 33 (2015) pp. 719–724.
[23] N. Jain and A. S. Sharma, "Evolution of electron current sheets in collisionless magnetic reconnection," Phys. Plasmas **22**, 102110 (2015).
[24] J. E. Stawarz, J. P. Eastwood, T. D. Phan, I. L. Gingell, M. A. Shay, J. L. Burch, R. E. Ergun, B. L. Giles, D. J. Gershman, O. Le Contel, P.-A. Lindqvust, C. T. Russell, R. J. Strangeway, R. B. Torbert, M. R. Argall, D. Fischer, W. Magnes, and L. Franci, "Properties of the turbulence associated with electron-only magnetic reconnection in Earth's magnetosheath," AstroPhys. J. Lett. **877**, L37 (2019).
[25] H. Y. Man, M. Zhou, Y. Y. Yi, Z. H. Zhong, A. M. Tian, X. H. Deng, Y. Khotyaintsev, C. T. Russell, and B. L. Giles, "Observations of electron-only magnetic reconnection associated with macroscopic magnetic flux ropes," Geophys. Res. Lett. **47**, e2020GL089659 (2020).
[26] P. S. Pyakurel, M. A. Shay, T. D. Phan, W. H. Matthaeus, J. F. Drake, J. M. TenBarge, C. C. Haggerty, K. G. Klein, P. A. Cassak, T. N. Parashar, M. Swisdak, and A. Chasapis, "Transition from ion-coupled to electron-only reconnection: basic physics and implications for plasma turbulence," Phys. Plasmas **26**, 082307 (2019).
[27] A. Mallet, "The onset of electron-only reconnection," J. Plasma Phys. **86** (2020).
[28] F. Califano, S. S. Cerri, M. Faganello, D. Laveder, M. Sisti, and M. W. Kunz, "Electron-only reconnection in plasma turbulence," Frontiers in

Physics **8**, 317 (2020).
[29]C. Vega, V. Roytershteyn, G. L. Delzanno, and S. Boldyrev, "Electron-only reconnection in kinetic-alfvén turbulence," Astrophysical J. Lett. **893**, L10 (2020).
[30]S. Lu, Q. Lu, R. Wang, P. L. Pritchett, M. Hubbert, Y. Qi, K. Huang, X. Li, and C. T. Russell, "Electron-Only Reconnection as a Transition From Quiet Current Sheet to Standard Reconnection in Earth's Magnetotail: Particle-In-Cell Simulation and Application to MMS Data," Geophys. Res. Lett. **49**, e2022GL098547 (2022).
[31]L. Franci, E. Papini, A. Micera, G. Lapenta, P. Hellinger, D. Del Sarto, D. Burgess, and S. Landi, "Anisotropic electron heating in turbulence-driven magnetic reconnection in the near-sun solar wind," Astrophys. J. **936**, 27 (2022).
[32]C. Granier, E. Tassi, D. Laveder, T. Passot, and P. L. Sulem, "Influence of ion-to-electron temperature ratio on tearing instability and resulting subion-scale turbulence in a low-βe collisionless plasma," Phys. Plasmas **31** (2024).
[33]H. Betar, D. Del Sarto, M. Ottaviani, and A. Ghizzo, "Multiparametric study of tearing modes in thin current sheets," Physics of Plasmas **27**, 102106 (2020).
[34]A. A. Schekochihin, S. C. Cowley, W. Dorland, G. W. Hammett, G. G. Howes, E. Quataert, and T. Tatsuno, "Astrophysical gyrokinetics: kinetic and fluid turbulent cascades in magnetized weakly collisional plasmas," Astrophys. J. Suppl. Series **182**, 310 (2009).
[35]B. N. Kuvshinov, E. Westerhof, T. J. Schep, and M. Berning, "Electron magnetohydrodynamics of magnetized inhomogeneous plasmas," Phys. Lett. A **241**, 287 (1998).
[36]N. Jain, J. Büchner, and P. A. Muñoz, "Nonlinear evolution of electron shear flow instabilities in the presence of an external guide magnetic field," Phys. Plasmas **24** (2017).
[37]N. Jain, A. von Stechow, P. A. Muñoz, J. Büchner, O. Grulke, and T. Klinger, "Electron-magnetohydrodynamic simulations of electron scale current sheet dynamics in the Vineta. II guide field reconnection experiment," Phys. Plasmas **24** (2017).
[38]A. Bohlin, A. von Stecho, K. Rahbarnia, O. Grulke, and T. Klinger, "Vineta ii: A linear magnetic reconnection experiment," Rev. Sci. Instrum. **85**, 023501 (2014).
[39]G. Kamelander and Y. I. Kolesnichenko, "Localized whistler eigenmodes in tokamaks," Phys. Plasmas **3**, 4102 (1996).
[40]P. Aleynikov and B. Breizman, "Stability analysis of runaway-driven waves in a tokamak," Nucl. Fus. **55**, 043014 (2015).
[41]Spong, D. A. and Heidbrink, W. W. and Paz-Soldan, C. and Du, X. D. and Thome, K. E. and Van Zeeland, M. A. and Collins, C. and Lvovskiy, A. and Moyer, R. A. and Austin, M. E. and Brennan, D. P. and Liu, C. and Jaeger, E. F. and Lau, C., "First direct observation of runaway-electron-driven whistler waves in tokamaks," Phys. Rev. Lett. **120**, 155002 (2018).
[42]W. Z. Zhang, H. S. Fu, J. B. Cao, Z. Wang, W. D. Fu, Y. Y. Liu, and Y. Yu, "First determination of whistler wave dispersion relation in superhot (t e> 5 kev) plasmas," Phys. Rev. Res. **6**, L012047 (2024).
[43]T. Fülöp, H. M. Smith, and G. Pokol, "Magnetic field threshold for runaway generation in tokamak disruptions," Phys. Plasmas **16** (2009).
[44]Z. Guo, C. J. McDevitt, and X.-Z. Tang, "Control of runaway electron energy using externally injected whistler waves," Phys. Plasmas **25** (2018).
[45]J. W. Connor and R. J. Hastie, "Relativistic limitations on runaway electrons," Nucl. Fus. **15**, 415 (1975).
[46]A. H. Boozer, "Runaway electrons and iter," Nucl. Fus. **57**, 056018 (2017).
[47]B. N. Breizman, P. Aleynikov, E. M. Hollmann, and M. Lehnen, "Physics of runaway electrons in tokamaks," Nucl. Fus. **59**, 083001 (2019).
[48]O. Z. Zabaidullin and V. V. Vikhrev, "Joule heating of a current layer due to plasma density inhomogeneities," Phys. Plasmas **3**, 2248–2254 (1996).
[49]T. Fülöp, G. Pokol, P. Helander, and M. Lisak, "Destabilization of magnetosonic-whistler waves by a relativistic runaway beam," Phys. Plasmas **13** (2006).
[50]M. Hata, H. Sakagami, and A. Das, "Kinetic simulation of electron transport using electron magnethydrodynamic structures," in *J. Phys.: Conf. Series*, Vol. 688 (2016) p. 012027.
[51]N. Attico, F. Califano, and F. Pegoraro, "Charge separation effects in electron-magnetohydrodynamic reconnection," Phys. Plasmas **16**, 2381–2387 (2000).
[52]D. Del Sarto, F. Califano, and F. Pegoraro, "Electron parallel compressibility in the nonlinear development of two-dimensional magnetohydrodynamic reconnection," Mod. Phys. Lett. B **20**, 931–961 (2006).
[53]M. Y. Yu and L. Stenflo, "Magnetic surface wave instabilities in plasmas," Phys. Fluids **28**, 3447–3449 (1985).
[54]A. M. Mirza and P. K. Shukla, "Magnetic electron drift vortex modes with the ion dynamics," Physics of Plasmas **4**, 2302–2304 (1997).
[55]P. Shukla and L. Stenflo, "Electron magnetohydrodynamics of inhomogeneous plasmas," Physics Letters A **259**, 49–52 (1999).
[56]R. L. Stenzel, "Whistler waves with angular momentum in space and laboratory plasmas and their counterparts in free space," Advances in Physics: X **1**, 687–710 (2016).
[57]M. Kono and H. L. Pécseli, "Cascade conditions in electron magnetohydrodynamic turbulence," Physics of Plasmas **29**, 122305 (2022).
[58]J. G. Turner and T. J. M. Boyd, "Parametric decay of whistler waves," Phys. Scripta **14**, 175 (1976).
[59]G. Murtaza and P. K. Shukla, "Decay of a whistler," Phys. Lett. A **104**, 382 (1984).
[60]L. Stenflo and G. Brodin, "Parametric decay of whistler waves in electron magnetohydrodynamics," Phys. Scripta **83**, 035503 (2011).
[61]T. M. Abdalla, B. N. Kuvshinov, T. J. Schep, and E. Westerhof, "Electron vortex generation by strong, localized plasma heating," Phys. Plasmas **8**, 3957 (2001).
[62]S. I. Braginskii, "Transport processes in a plasma," Reviews of Plasma Physics **1**, 205 (1965).
[63]J. D. Huba, *NRL Plasma Formulary* (Naval Research Laboratory, Washington, DC, 2007 (revised)).
[64]F. Porcelli, D. Borgogno, F. Califano, D. Grasso, M. Ottaviani, and F. Pegoraro, "Recent advances in collisionless magnetic reconnection," Plasma Phys. Controll. Fusion **44**, B389 (2002).
[65]D. Del Sarto, F. Pucci, A. Tenerani, and M. Velli, ""ideal" tearing and the transition to fast reconnection in the weakly collisional MHD and EMHD regimes," J. Geophys. Res.- Space Phys. **121**, 1857–1873 (2016).
[66]H. Cai and D. Li, "Magnetic reconnection with electron viscosity in electron magnetohydrodynamics," Phys. Plasmas **15**, 032301 (2008).
[67]H. Furth., "Instabilities due to finite resistivity or finite current-carrier mass," in *Proceedings of the "Enrico Fermi" international school of Physics of the Italian Physical Society, Course XXV. Advanced plasma Theory*, edited by Marshall N. Rosenbluth (Academic Press, 1962) p. 159.
[68]M. J. Martin, W. Gekelman, B. Van Compernolle, P. Pribyl, and T. Carter, "Experimental observation of convective cell formation due to a fast wave antenna in the large plasma device," Phys. Rev. Lett. **119**, 205002 (2017).
[69]F. Brochard, D. Geneve, S. Heuraux, D. Bobkov, D. Del Sarto, E. Faudot, A. Ghizzo, E. Gravier, N. Lemoine, M. Lesur, N. Louis, J. Moritz, T. Reveillé, V. Rohde, U. Stroth, G. Urbanczyk, F. Volpe, and H. Zohm, "Spektre, a linear radiofrequency device for investigating edge plasma physics," (IAEA Publications, 2010) pp. THS/P5–03.
[70]V. Mukhovatov, M. Shimada, A. N. Chudnovskiy, C. A. E., Y. Gribov, G. Federici, A. S. Kardaun, O. Kukushkin, A. Polevoi, V. D. Pustovitov, Y. Shimomura, T. Sugie, M. Sugihara, and G. Vayakis, "Overview of physics basis for ITER," Plasma Phys. Controll. Fusion **45**, A235–A252 (2003).
[71]T. Rafiq, Z. Wang, S. Morosohk, E. Schuster, J. Weiland, W. Choi, and H.-T. Kim, "Validating the multi-mode model's ability to reproduce diverse tokamak scenarios," Plasma **6**, 435 (2023).
[72]B. Na, A. Robbins, J. Yoo, and J. H., "Double-sided electron energy analyzer for measurement of non-maxwellian electron energy distributions," Rev. Sci. Instrum. **94**, 123509 (2023).
[73]I. Furno, T. Intrator, E. Torbert, C. Carey, M. D. Cash, J. K. Campbell, W. J. Fienup, C. A. Werley, and G. A. Wurden, "Reconnection scaling experiment: A new device for three-dimensional magnetic reconnection studies," Rev. Sci. Instr. **74**, 2324 (2003).
[74]V. H. Hansteen and M. Velli, "Solar wind models from the chromosphere to 1*au*," Space Sci. Rev. **172**, 89 (2012).
[75]S. Esteban Pozuelo, A. Asensio Ramos, J. de la Cruz Rodriguez, J. Trujillo Bueno, and M. J. Martinez Gonzalez, "Estimating the longitudinal magnetic field in the chromosphere of quiet-Sun magnetic concentrations," Astronomy and Astophysics **672**, A141 (2023).
[76]D. Verscharedn, K. G. Klein, and B. A. Maruca, "The multi-scale nature of the soalar wind," Living Rev. Solar Phys. **16**, 5 (2019).

[77]M. Moncuquet, N. Meyer-Vernet, K. Issautier, M. Pulupa, J. W. Bonnell, S. D. Bale, T. D. de Wit, K. Goetz, L. Griton, P. R. Harvey, R. J. MacDowall, M. Maksimovic, and D. M. Malaspina, "First in situ measurements of electron density and temperature from quasi-thermal noise spectroscopy with Parker solar probe/Fields," Astrophys. J. Suppl. Series **246**, 44 (2020).
[78]D'Amicis, R. and Perrone, D. and Bruno, R. and Velli, M., "On Alfvénic slow wind: a journey from the Earth back to the Sun," J. Geophys. Res. −Space Phys. **126**, e2020JA028996 (2021).
[79]S. V. Bulanov and A. S. Pegoraro, F. andSakharov, "Magnetic recoonection in electron magnetohydrodynamics," Phys. Fluids **8**, 2499–2508 (1992).
[80]A. Fruchtman and H. R. Strauss, "Modification of short scale-length tearing modes by the hall field," Phys. Fluids B **5**, 1408 (1993).
[81]N. Attico, F. Califano, and F. Pegoraro, "Forced magnetic field line reconnection in electron magnetohydrodynamics," Phys. Plasmas **5**, 2849 (1998).
[82]Shaikhislamov, I. F., " Hall dynamics and resistive tearing instability ," J. Plasma Phys. **70**, 599 (2004).
[83]Shaikhislamov, I. F., " Collapse of the neutral current sheet and reconnection at micro-scales ," J. Plasma Phys. **74**, 215 (2008).
[84]H. Betar, D. Del Sarto, M. Ottaviani, and A. Ghizzo, "Multiparametric study of tearing modes in thin current sheets," Phys. Plasmas **27**, 102106 (2020).
[85]D. Del Sarto, F. Califano, and F. Pegoraro, "Current layer cascade in collisionless electron magnetohydrodynamic reconnection and electron compressibility effects," Phys. Plasmas **12**, 012317 (2005).
[86]D. Medina-Roque and Y.-C. Lin, *Plasma parameters and potential experiments analysis for the Sheath, Plasma Edge Kinetic Turbulence Radiofrequency Experiment (SPEKTRE)*, Université de Lorraine, Institut Jean Lamour, Nancy, France (2020), Master I Internship report.